Tectonics®

RESEARCH ARTICLE
10.1029/2023TC008013

Key Points:

- Tectonic evolution of the Eastern Southern Alps
- Long-lived orogenic deformation in the Alps
- Cretaceous far field tectonics, multiple (re)activation, and out-of-sequence thrusting constrained through K-Ar and U-Pb dating

Supporting Information:

Supporting Information may be found in the online version of this article.

Correspondence to:

M. Curzi and G. Viola,
manuel.curzi@uniroma1.it;
giulio.viola3@unibo.it

Citation:

Curzi, M., Viola, G., Zuccari, C., Aldega, L., Billi, A., van der Lelij, R., et al. (2024). Tectonic evolution of the Eastern Southern Alps (Italy): A reappraisal from new structural data and geochronological constraints. *Tectonics*, *43*, e2023TC008013. https://doi.org/10.1029/2023TC008013

Received 17 JULY 2023
Accepted 18 FEB 2024

Author Contributions:

Conceptualization: Manuel Curzi, Giulio Viola, Costantino Zuccari, Gianluca Vignaroli
Data curation: Manuel Curzi, Giulio Viola, Costantino Zuccari, Gianluca Vignaroli
Formal analysis: Manuel Curzi, Costantino Zuccari, Luca Aldega, Andrea Billi
Funding acquisition: Giulio Viola
Investigation: Manuel Curzi, Giulio Viola, Costantino Zuccari, Andrea Billi, Roelant van der Lelij, Andrew Kylander-Clark, Gianluca Vignaroli
Methodology: Manuel Curzi, Luca Aldega, Roelant van der Lelij, Andrew Kylander-Clark

Tectonic Evolution of the Eastern Southern Alps (Italy): A Reappraisal From New Structural Data and Geochronological Constraints

Manuel Curzi[1,2], Giulio Viola[1], Costantino Zuccari[1,3], Luca Aldega[2], Andrea Billi[4], Roelant van der Lelij[5], Andrew Kylander-Clark[6], and Gianluca Vignaroli[1]

[1]Dipartimento di Scienze Biologiche, Geologiche ed Ambientali–BiGeA, Università di Bologna, Bologna, Italy, [2]Dipartimento di Scienze della Terra, Sapienza Università di Roma, Rome, Italy, [3]Dipartimento di Scienze della Terra, Università di Pisa, Pisa, Italy, [4]Consiglio Nazionale delle Ricerche, IGAG, Rome, Italy, [5]Geological Survey of Norway, Trondheim, Norway, [6]Department of Earth Science, University of California, Santa Barbara, CA, USA

Abstract The Eastern Southern Alps fold-and-thrust belt (ESA) is part of the seismically active S-verging retro-wedge of the European Alps. Its temporal tectonic evolution during continental shortening has so far been constrained by few and low-resolution indirect time constraints. Aiming at better elucidating the ESA spatiotemporal evolution, we gathered new structural and geochronological data from two regional thrust systems: the innermost south verging Valsugana Thrust (VT) and the more external Belluno Thrust System (BTS). Field work allowed us to constrain the geometry and kinematics of those thrusts and related folds and informed our sampling strategy to carry out fault gouge K-Ar and tectonic carbonate U-Pb dating from representative samples structurally associated with the VT and BTS. Our results suggest that the VT was active already in the Late Cretaceous (between ~78 and 76 Ma) in response to far-field stresses, with repeated reactivation continuing to the Late Miocene (~6 Ma). The BTS recorded two distinct deformation events during the Oligocene (~30 Ma) and at the Oligocene-Miocene boundary (~23 Ma). The VT was active for ~72 Myr and partly acted during out-of-sequence thrusting. Based on regional correlations, we propose that the ESA share a similar spatiotemporal deformation history with the central Southern Alps farther to the west. We suggest a conceptual regional tectonic model wherein multiple, broadly coeval deformation events occurred in the entire Southern Alps during their long-lived orogenic deformation in response to generally continuous NW-SE shortening.

1. Introduction

Fold-and-thrust belts (FTBs) accommodate significant shortening of the Earth's crust during deformation histories that can last up to several dozens of millions of years (e.g., Lacombe & Bellahsen, 2016; Lacombe et al., 2007). The analysis of their geometry and kinematic framework, including their late orogenic extension, is key to the refined understanding of first-order tectonic concepts and their successful modeling (e.g., Lacombe & Beaudoin, 2023; Lacombe et al., 2007, 2021; Pana & van der Pluijm, 2015; Tavani et al., 2015). In addition, given that their tectonic evolution is commonly associated with fluid migration and/or formation of ore deposits at the regional scale, FTBs are crucial to the analysis of petroleum plays, mineral deposits, and geothermal field distribution (e.g., Beaudoin et al., 2022; Evans & Fischer, 2012; Harding & Lowell, 1979; Mitra, 1986). Seismicity, moreover, is intimately associated with active FTBs such that they are not only of great scientific interest, but also of large direct relevance to society (e.g., Lacombe et al., 2007).

It is now well acknowledged that the final, deformed state of FTBs may be reached via multiple kinematic paths of their constituent thrust sheets, whereby continuous versus episodic deformation during their emplacement can represent possible scenarios (e.g., Lacombe et al., 2007). Conceptual models show that thrust sheets commonly have progressively younger, generally non-overlapping emplacement ages from the hinterland to the foreland (e.g., Barchi et al., 1998; Boyer & Elliott, 1982). More complex patterns of deformation, however, are being increasingly recognized by means of high-resolution structural, stratigraphic and geophysical studies (e.g., Burbank et al., 1992; Hudec & Davis, 1989; Morley, 1988). In fact, a broader and non-linear distribution of deformation in space and time is now identified even in "classic" break-forward thrust belts as documented, for instance, in the Rocky Mountains of Canada (e.g., DeCelles, 1994). As a result, there is a growing appreciation that the kinematic framework of FTBs can be temporally and spatially complex, recording long-lived and

Project administration: Giulio Viola
Software: Manuel Curzi, Roelant van der Lelij, Andrew Kylander-Clark
Supervision: Giulio Viola, Gianluca Vignaroli
Validation: Manuel Curzi, Giulio Viola, Luca Aldega, Andrea Billi, Gianluca Vignaroli
Visualization: Manuel Curzi, Andrea Billi
Writing – original draft: Manuel Curzi, Giulio Viola, Costantino Zuccari, Luca Aldega, Andrea Billi, Roelant van der Lelij, Andrew Kylander-Clark, Gianluca Vignaroli
Writing – review & editing: Manuel Curzi, Giulio Viola, Costantino Zuccari, Luca Aldega, Andrea Billi, Gianluca Vignaroli

multiphase deformation histories in their stratigraphic, structural, metamorphic, and geochemical archive (e.g., Lacombe & Bellahsen, 2016; Lacombe et al., 2007, 2021; Pana & van der Pluijm, 2015). Constraining the timing of deformation is, therefore, of primary importance for the in depth understanding of their complex evolution. The spatial and temporal evolution of FTBs is generally constrained by magnetostratigraphic, stratigraphic and subsurface seismic studies (e.g., Cavinato & Celles, 1999; Cipollari & Cosentino, 1995). This approach, however, may at times lack sufficient accuracy to provide tight temporal constraints, limiting the possibility to accurately model the propagation of deformation fronts within FTBs and fully understand their seismicity through space and time.

Faulting in FTBs is generally assisted by fluids that promote precipitation of syn-kinematic clay minerals in fault rocks and tectonic mineralizations such as cement in fault breccias, vein networks, and slickenfibers (e.g., Boullier et al., 2004; Goodfellow et al., 2017; Sibson, 1994; Sibson et al., 1975; Van der Pluijm et al., 2001; Vrolijk & van der Pluijm, 1999). Direct dating of these tectonic mineralizations makes it possible to constrain the timing of fault activity and represents a powerful tool to unravel complex and long-lived tectonic histories. Indeed, it is now well acknowledged that U-Pb dating of tectonic carbonates (*sensu* Müller, 2003) and Ar/Ar or K-Ar dating of syn-kinematic clay minerals allow constraining brittle deformation events both at the local (e.g., initiation, reactivation, and longevity of one individual fault; e.g., Clauer, 2013; Torgersen et al., 2015; Nuriel et al., 2017; Hansman et al., 2018; Zwingmann et al., 2004; Viola et al., 2013; Pana and Van der Pluijm, 2015; Goodfellow et al., 2017; Mottram et al., 2020; Craddock et al., 2022; Curzi et al., 2021; Munoz-Lopez et al., 2022; Vignaroli et al., 2022; Roberts & Holdsworth, 2022) and regional scale, as convincingly demonstrated for the Oman Mountains (Carminati et al., 2020), Scandinavian Caledonides in Norway (Torgersen et al., 2015), Rocky Mountains in Canada (Pana and Van der Plujim, 2015), Bohemian Massif (Roberts et al., 2021), Chicomuselo fold-and-thrust belt in Mexico (Palacios-Garcia et al., 2023), Iberian Chain in Spain (Aldega et al., 2019; Cruset et al., 2020; Haines and Van del Plujim, 2023), the Apennines in Italy (Smeraglia et al., 2019, Viola et al., 2018, 2022; Carboni et al., 2020; Curzi et al., 2020a, 2020b, Curzi, Cipriani, et al., 2024; Tavani et al., 2023), and the Western Alps (Bilau et al., 2023; Looser et al., 2021; Smeraglia et al., 2021).

The Eastern Southern Alps (ESA) of the European Alps represent an excellent natural laboratory where to study the tectonic evolution of a complex and active FTB. Despite the efforts invested so far by the scientific community to assess the seismogenesis of the ESA (e.g., D'Agostino et al., 2005; Galadini et al., 2005; Anselmi et al., 2011; Bignami et al., 2012; Cheloni et al., 2014; Danesi et al., 2015; Viganò et al., 2015; Serpelloni et al., 2016; Anderlini et al., 2020; Picotti et al., 2022), their long-lived tectonic evolution remains mostly constrained by structural and stratigraphic data. Such data have been used since the '90s to document that the ESA stem from a series of distinct tectonic phases ensued from the Cretaceous to the Neogene in response to different paleostress field orientations (e.g., Caputo et al., 2010; Castellarin & Cantelli, 2000; Castellarin et al., 2006; Selli, 1998; Venzo, 1939). Only in more recent times, thermochronological studies have provided quantitative constraints on thrusting-associated (i.e., vertical displacement-related) exhumation within the ESA during the Oligocene-Miocene (Heberer et al., 2017; Zattin et al., 2003, 2006). The lack of other and more accurate geochronological constraints directly associated with thrusting in the ESA has precluded thus far the possibility to validate or strengthen existing evolutionary models and provide a detailed reconstruction of the regional Alpine deformation through space and in an absolute time perspective.

With this study we aim at providing new and much needed time constraints on thrust activity and draw a model of geochronologically-constrained tectonic evolution for the ESA. To this end, we have investigated key exposures along two regional thrusts systems in the ESA and coupled (a) mesoscale structural observations and kinematic analysis of representative tectonic structures, (b) microtextural characterizations and U-Pb dating of tectonic carbonates, and (c) K-Ar dating of authigenic/syn-kinematic clay minerals from structurally constrained fault gouges.

Our results, in addition to confirming the overall SE vergence of the ESA, constrain the onset of Alpine deformation therein to the Late Cretaceous, when the first top-to-the SE thrusting-related deformation increments localized at low structural levels in response to far-field stresses. Our structural and geochronological constraints are compatible with overall NW-SE crustal shortening accommodated by repeated top-to-the SE thrust (re)activation spanning a time span of ∼73 Ma. Ages of thrust (re)activation in the ESA partially overlap with the age of compression in the central Southern Alps (cSA), calling for a tentative reappraisal of the long-term tectonic evolution of the entire S-verging domain of the European Alps.

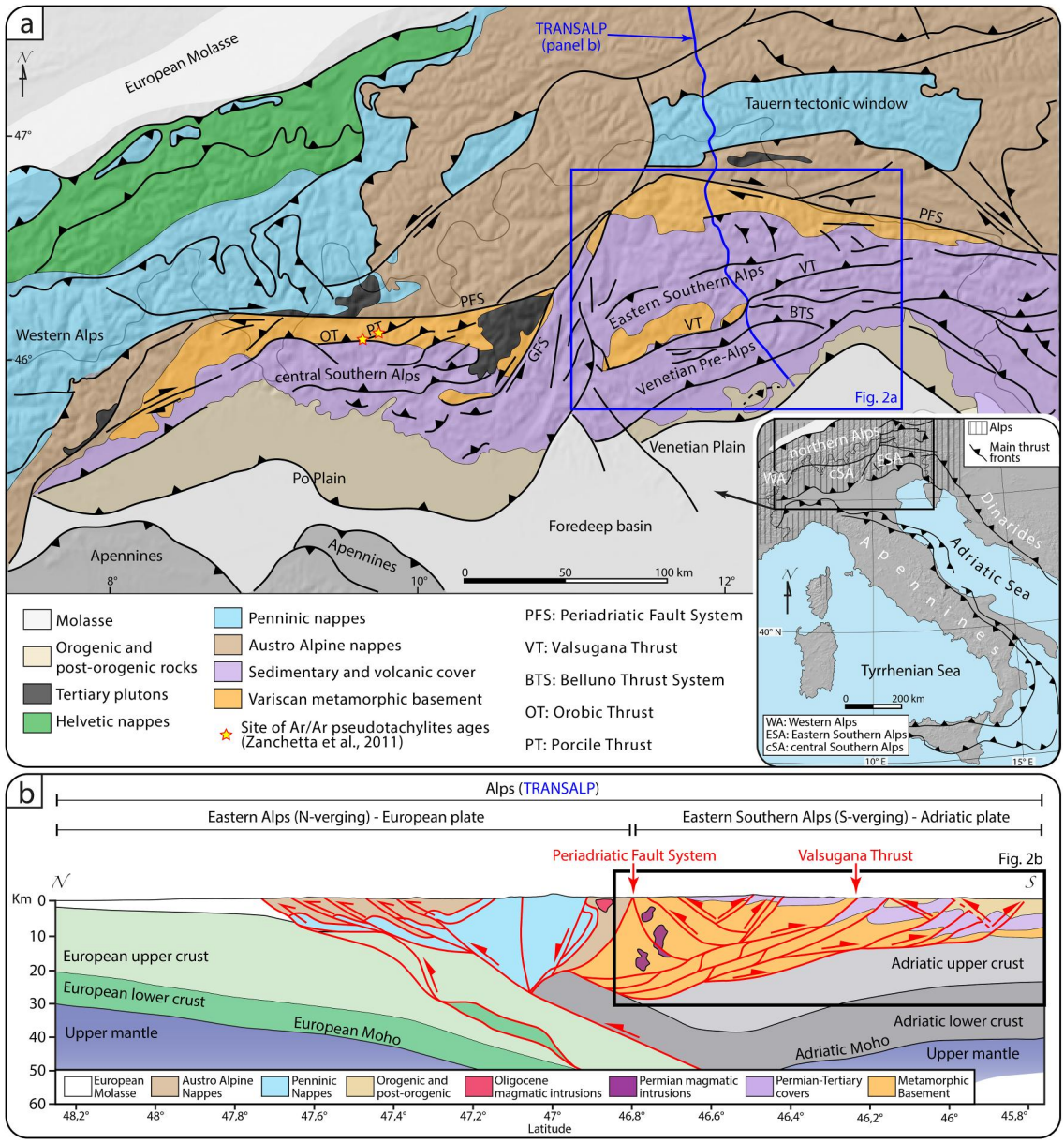

Figure 1. (a) Schematic geological map of the Alps (modified after Bigi et al., 1989). The trace of the TRANSALP seismic profile is shown. (b) Crustal structure of the Alps inferred from the TRANSALP seismic profile (redrawn and modified from Castellarin et al., 2006).

2. Geological Setting

2.1. The Central and Eastern Southern Alps

The Southern Alps (SA) belong to the Alpine chain (Figure 1a), which formed in response to the Cretaceous-Paleogene closure of an eastern branch of the Alpine Tethys (and the associated convergence between the European and Adriatic plates) and continued to build-up during the Europe-Adria continental collision in the uppermost Eocene (Carminati & Doglioni, 2012; Handy et al., 2010). The SA are located to the south of the ~ E-W orogen-scale Periadriatic Fault System, the most striking tectonic boundary of the entire Alpine chain that separates the N- and Europe-verging Alps to the north from the S-verging SA to the south (e.g., Handy et al., 2010; Muller et al., 2001; Schmid et al., 1989, Figures 1a and 1b). The SA are divided into two parts by the left-lateral transpressive Giudicarie Fault System (GFS; e.g., Castellarin et al., 2006; Viola et al., 2001, Figure 1a). To the west and east of the GFS, the SA are represented by the cSA and the ESA, respectively (Figure 1a). The cSA

10.1029/2023TC008013

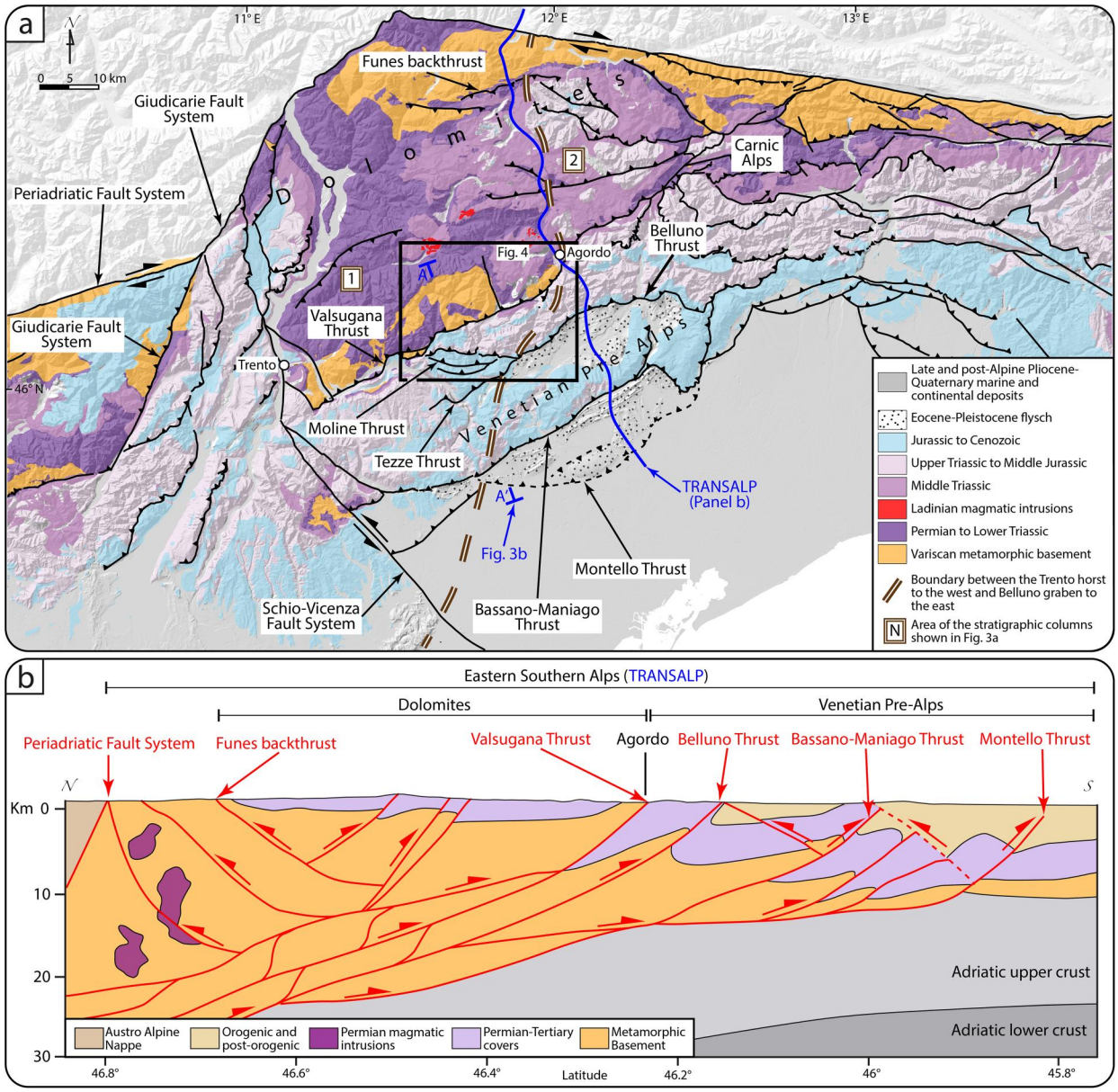

Figure 2. (a) Geological map of the Eastern Southern Alps (ESA) showing the main faults (redrawn and modified from Curzi et al., 2023; after Mietto et al., 2020). The trace of the TRANSALP seismic profile is shown. (b) Detail of the crustal structure of the ESA, including the Dolomites and Venetian Pre-Alps, inferred from the TRANSALP seismic profile (redrawn and modified from Castellarin et al., 2006; Curzi et al., 2023).

consist of a thick-skinned FTB where the Variscan metamorphic basement thrusted over the Permian-Cenozoic cover succession along the ~80 km long and NE-SW striking Orobic Thrust (OT) and the associated Porcile Thrust (PT; Figure 1a). The OT and PT first activated during the Late Cretaceous, but were later reactivated during the middle Eocene before being finally cut by late Eocene magmatic bodies (D'Adda et al., 2011; Zanchetta et al., 2011, 2015, Figure 1a). During the Neogene, orogenic deformation in the cSA propagated toward the south, leading to the formation of frontal thrusts that are currently buried beneath the Po Plain (Zanchetta et al., 2015, Figure 1a).

The ESA are bounded by the GFS to the west and the Dinarides to the east (Castellarin et al., 2006; Doglioni & Carminati, 2008; Schmid et al., 2008, Figures 1a and 2a). The ESA were influenced by several tectonic and magmatic events, including: (a) Permian-Triassic rifting that caused lithospheric thinning and magmatism and the

development of N-S trending basins and structural highs (among them, the Atesina Platform to the west and the Carnico-Bellunese Basin to the east; Bosellini & Doglioni, 1986; Cassinis et al., 2008; Doglioni, 1987; Morelli et al., 2012), (b) Middle Triassic strike-slip tectonics that caused differential subsidence within the SA and that climaxed with a magmatic event of Ladinian age (Bonadiman et al., 1994; Castellarin et al., 1998; Doglioni & Carminati, 2008; Lustrino et al., 2019; Sloman, 1989), (c) Late Triassic-Middle Jurassic rift-related extensional tectonics that led to the development of the ∼ N-S trending Trento horst in the western side of the ESA and Belluno graben in the eastern side of the ESA and climaxed during the Early-Middle Jurassic with the opening of the Ligurian-Piedmont Ocean (Carminati et al., 2010; Cozzi, 2002; Handy et al., 2010; Masetti et al., 2012; Picotti & Cobianchi, 2017; Trombetta & Bottoli, 1998), and, finally, (d) several Alpine compressional phases, including a Late Cretaceous-Paleocene phase during the subduction of the Alpine Tethys, an Eocene phase associated with the present-day continental margin collision, and an Eocene-Pliocene post-collisional phase (Caputo et al., 2010; Castellarin & Cantelli, 2000; Castellarin et al., 2006; Doglioni & Bosellini, 1987; Keim & Stingl, 2000). It has been proposed that the Eocene-Pliocene post-collisional evolution of the ESA led to three distinct regional structural systems, which are (a) the compressional Eocene-Miocene Dinaric system, accommodating shortening in response to overall NE-SW compression, (b) the compressional Miocene Valsugana system, characterized by structures formed in response to NNW-SSE compression, and (c) the transpressional Miocene-Pliocene Schio-Vicenza system that accommodated WNW-ESE compression (Castellarin & Cantelli, 2000; Castellarin et al., 2006). Among these, the NNW-SSE shortening attributed to the Miocene Valsugana system of Castellarin and Cantelli (2000) and Castellarin et al. (2006) is thought to be the main driver behind the current geometric and kinematic structural framework of the Dolomites. This framework was shaped by kilometric shortening along NE-SW striking and SE-verging thrusts and, to a lesser extent, along NW-verging backthrusts and minor strike-slip and transpressional faulting (e.g., Curzi et al., 2023; Doglioni, 1987; Doglioni & Carminati, 2008; Schönborn, 1999, Figures 2a and 2b). NNW-SSE compression is still active at the scale of the belt, as documented by historical and present-day seismicity, leading to shortening in the southernmost frontal portion of the Dolomites and along the Venetian Pre-Alps (Anderlini et al., 2020; Anselmi et al., 2011; Bignami et al., 2012; Cheloni et al., 2014; Galadini et al., 2005; Serpelloni et al., 2016; Viganò et al., 2015).

2.2. Stratigraphic Framework of the Eastern Southern Alps

In the ESA, a ∼5–6 km thick volcanic and sedimentary cover, which is part of the Trento horst to the west and Belluno graben to the east, rests atop a Paleozoic metamorphic basement (Figures 2a and 3a, Doglioni & Neri, 1988; Doglioni & Carminati, 2008). In the western ESA, the cover consists of Permian ignimbrite, continental sandstone of the Arenaria della Val Gardena Fm., carbonate and evaporite of the Bellerophon Fm., and Upper Permian-Lower Triassic terrigenous carbonate of the Werfen Fm. The overlying Triassic succession consists of conglomerate and carbonate of the Undifferentiated Anisian Complex (Massironi et al., 2007), platform carbonate of the Sciliar Fm., its Livinallongo Fm. heteropic basinal sequence, Ladinian volcanic products, platform carbonate of the Upper Triassic Cassian Dolomite Fm., its coeval San Cassiano Fm. basinal sequence counterpart, and the platform carbonate of the Dolomia Principale Fm. From the Lower Jurassic, the platform and shallow water carbonate of the Calcari Grigi Group sedimented on top of the Trento horst (western side of the ESA; Figures 2a and 3), while the basinal marly and cherty carbonate of the Igne and Soverzene fms. deposited in the Belluno graben (eastern side of the ESA; Figures 2a and 3a). The Middle-Upper Jurassic succession in the Trento horst is made up of the marly and cherty limestone of the Rosso Ammonitico Fm., while in the Belluno graben it is represented by the calcarenite of the Vajont Limestone and marly and cherty carbonate of the Rosso Ammonitico Fm. The Trento horst and the Belluno graben were evened in the Early Cretaceous by the cherty pelagic limestone of the Maiolica Fm. above which rests the marl and marly and cherty limestone of the Scaglia Group (composed of the Lower-Upper Cretaceous Scaglia Variegata Alpina and the Upper Cretaceous-lower Eocene Scaglia Rossa fms.) and an overlying Paleocene-Miocene marly to terrigenous succession (Bosellini et al., 1981, 2003; Masetti et al., 2012; Picotti & Cobianchi, 2017; Stefani et al., 2007).

2.3. Tectono-Structural Framework of the Eastern Southern Alps

The ESA are deformed by NE-SW striking thrusts that formed and propagated from north to south (i.e., moving from the internal ESA toward the Venetian Plain foreland; e.g., Castellarin et al., 2006; Doglioni & Carminati, 2008, Figure 2a). Balanced cross sections constrain the total cumulative shortening for the whole ESA to ∼30–50 km (Castellarin et al., 2006; Doglioni, 1990; Schönborn, 1999). The most important thrust in the area is

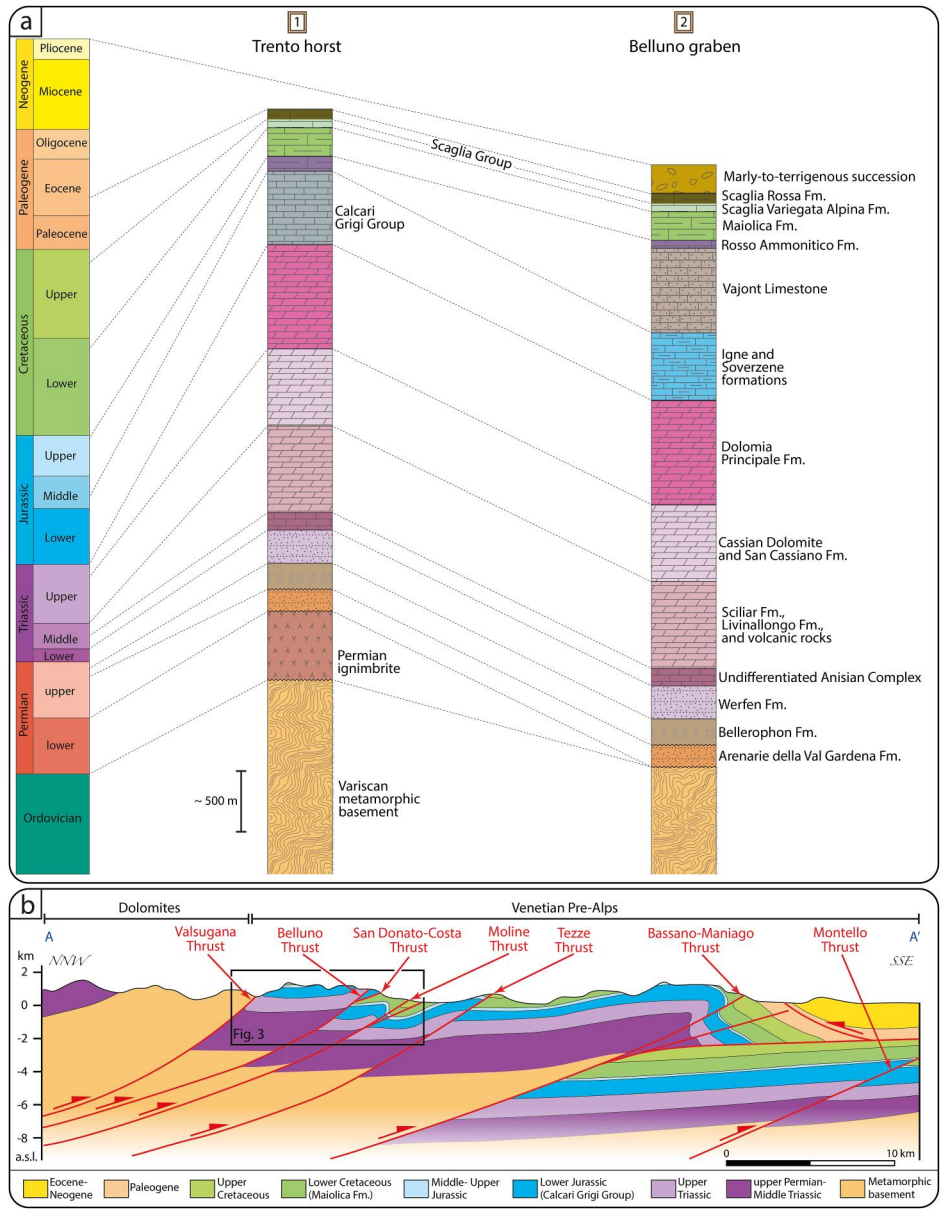

Figure 3. (a) Simplified stratigraphic columns for the Trento horst to the west and Belluno graben to the east (data from Masetti et al., 2012; Bosellini et al., 1981; D'Alberto et al.,1995; Picotti & Cobianchi, 2017; Stefani et al., 2007; Zuccari et al., 2021). The area of the stratigraphic columns is shown in Figure 2a. (b) Simplified cross-section along the Eastern Southern Alps (redrawn and modified from Schönborn, 1999; Doglioni & Carminati, 2008).

the SE-verging Valsugana Thrust (VT), which was active with different kinematics since Permian times (Bosellini & Doglioni, 1986; Brandner et al., 2011; Castellarin & Vai, 1982; Selli, 1998), and in the current geometric configuration separates the Dolomites *s.s.* to the north from the Venetian Pre-Alps to the south; it accommodated a cumulative shortening of ∼8–10 km during the Alpine orogenesis (e.g., Bosellini & Doglioni, 1986; Doglioni, 1987; Doglioni & Carminati, 2008; Selli, 1998, Figures 2 and 3b). The VT Alpine activity has been dated to the Serravallian-Tortonian (Middle Miocene) by stratigraphic constraints and apatite fission track thermochronology (Castellarin & Cantelli, 2000; Castellarin et al., 1992; Dunkl et al., 1996; Heberer et al., 2017; Selli, 1998; Venzo, 1939; Zattin et al., 2003, 2006). VT faulting caused the juxtaposition of the Variscan metamorphic basement and its sedimentary cover in the hanging wall against the sedimentary cover of the Venetian Pre-Alps (e.g., Bosellini & Doglioni, 1986; Doglioni, 1987). In its hanging wall, SE-verging thrusts and minor NW-verging backthrusts deform the basement and its overlying sedimentary cover (Figure 2). Minor

strike-slip and transpressional faults also formed within the Dolomites (Doglioni & Carminati, 2008) as expression of local Alpine transpressional stress conditions (Curzi et al., 2023).

In the footwall, the Neogene Venetian Pre-Alps are deformed by a series of regional-scale thrusts, which, from north to south, are the Belluno Thrust System (BTS), comprising the Belluno Thrust (BT) and the San Donato-Costa Thrust splay (SDCT), and the Moline, Tezze, Bassano-Maniago, and Montello thrusts, which variably deformed the Triassic-Miocene stratigraphic succession for a cumulative shortening of up to ∼30 km (e.g., Doglioni & Carminati, 2008; Picotti et al., 2022; Vignaroli et al., 2020; Zuccari et al., 2021, 2022, Figures 2 and 3b). Out of those, the southernmost and more external Bassano-Maniago and Montello thrusts are still seismically active, hosting hypocenters between 5 and 18 km deep within the sedimentary cover and metamorphic basement (e.g., Anderlini et al., 2020; Benedetti et al., 2000; Cheloni et al., 2014; Galadini et al., 2005, Figure 2b). Presently, no geochronological constraints exist on the activity of the major thrusts and the long-term tectonic evolution of the ESA, thus hampering the possibility of temporally scanning the sequence of tectonic events in this portion of the SA.

3. Study Area and Methods

Our field work and sampling focused along a broad ∼N-S transect in the central sector of the ESA that crosses the VT and BTS and their associated structures (Figure 4). In detail, we focused particularly on four representative outcrops that grant access to well exposed sections of the metamorphic basement and Triassic sedimentary cover along the VT, one structural station in the Lower Jurassic sedimentary succession along the BT, and one structural station within the Lower Cretaceous sedimentary cover along the SDCT (Figure 4). We combined detailed meso-structural analysis and structurally controlled sampling, microtextural characterization and U-Pb dating of tectonic carbonates, as well as X-ray diffraction and K-Ar dating of clay minerals separated from structurally constrained clay gouge samples (Figure 4). We performed U-Pb dating on sample material that was investigated by cathodoluminescence microscopy and that exhibited homogeneous luminescence. Hence, we interpret each dated tectonic carbonate as having precipitated from one single precipitation event at the sample scale, which makes it possible to interpret the U-Pb results in terms of faulting events. Details on the collected samples are provided in Figure 4 and are stored in the Figshare public repository (10.6084/m9.figshare.24550936), whereas the analytical methods are described in the supplementary material.

4. Results

In the following we provide a description of each studied structural station along the VT and BTS. Subsequently, we describe our microtextural observations and results from the geochronology study. To assist the reader while following the structural data, the sites of sampling and the geochronological results, Table 1 sums up the sampled material collected from the six structural stations described below.

4.1. Mesostructural Observations and Sampling Along the Valsugana Thrust

4.1.1. Structural Station n. 1 (Lat.: 46°16′12″N, Long.: 12°02′07″E; Figure 5)

The Paleozoic metamorphic basement is well exposed close to the town of Agordo, where it consists of greyish phyllites (Figure 5a). The metamorphic (Variscan) foliation is penetrative and marked by mica and stretched and transposed quartz veins. Four different folding events of Variscan and Alpine age are recognizable (Poli & Zanferrari, 1992, Figure 5b). While the first folding phase formed cm-scale isoclinal and commonly rootless folds associated with the main regional foliation, and the second a discrete crenulation cleavage during the Variscan deformation, the last two phases are more domainal and generally ascribed to Alpine shortening along the VT.

Two discrete ENE-WSW striking, 35–55° NNW dipping and SE-verging thrusts cut the basement rocks (Figure 5a). The lower thrust borders two distinct volumes of basement rocks, each with a differently oriented metamorphic foliation. In detail, thrust-parallel and thrust-orthogonal foliation planes are observed in its hanging wall and footwall, respectively (Figure 5a). In the hanging wall to the lower thrust, sigmoidal lithons are stretched parallel to the thrust transport direction indicating a top-to-the SE sense of movement, which is consistent with the VT regional transport. Lenses of fault gouge occur along the lower thrust, where sample VT6 has been collected (Figure 5c).

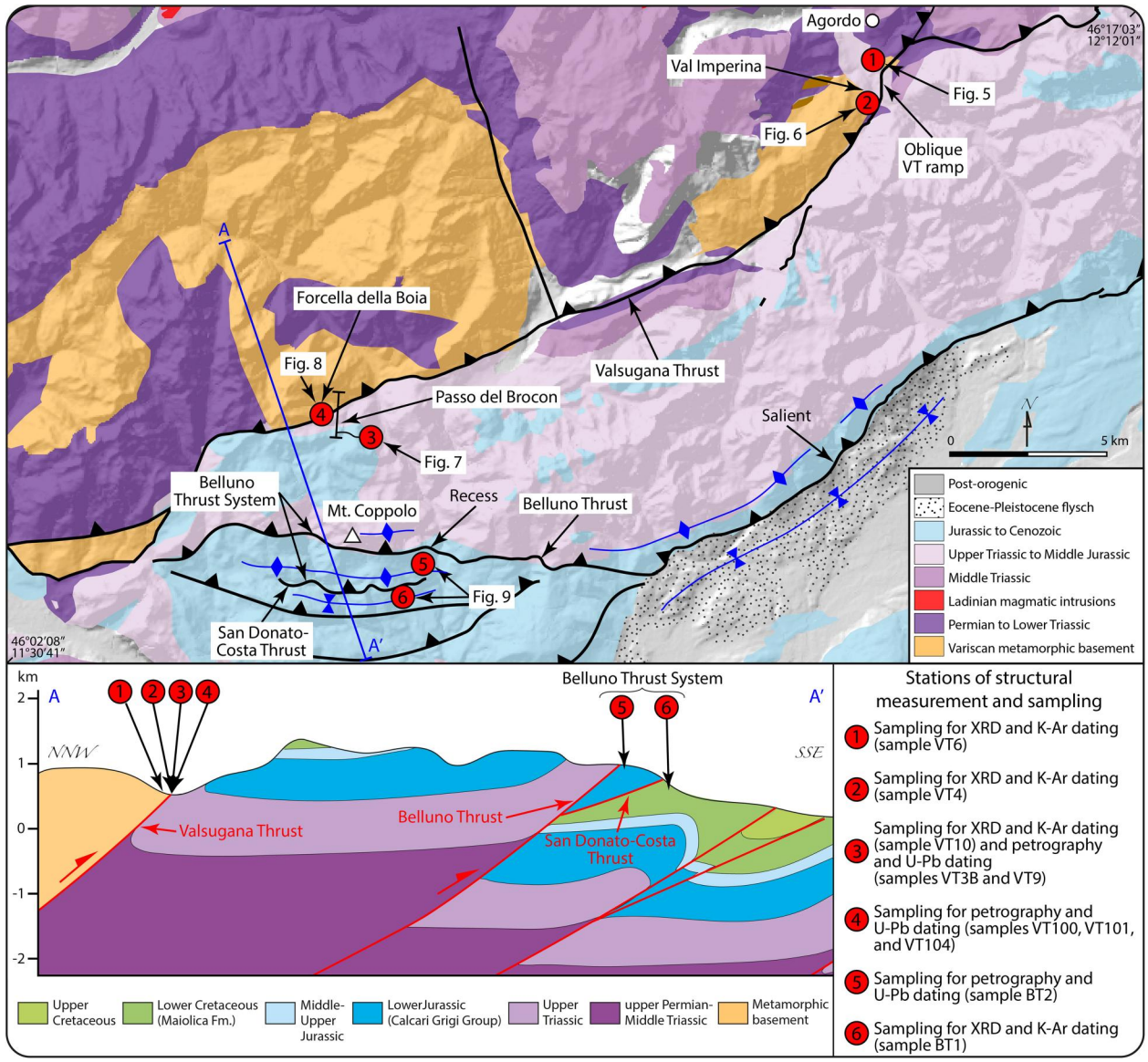

Figure 4. Simplified geological map (enlarged from Figure 2a; after Mietto et al., 2020) and representative cross-section of the studied sector of the Eastern Southern Alps. The location of the studied structural stations and sampling sites along the Valsugana Thrust and Belluno Thrust System is shown on the map and projected along the cross-section.

4.1.2. Structural Station n. 2 (Lat.: 46°15′08″N, Long.: 12°02′17″E; Figure 6)

In Val Imperina, ~1 km to the south of structural station n.1, the metamorphic basement is juxtaposed directly onto the Upper Triassic shallow water carbonate of the Dolomia Principale Fm (Figure 6a). In map view, this exposure is located close to a NNE-SSW striking segment of the VT (Figure 4). The well-exposed carbonate of the footwall is affected by tectonic structures related to four distinct deformation phases (herein referred to as D_1–D_4; Figure 6a), which are described below and whose relative timing is inferred based on their mutual and systematic crosscutting relationships observed at the outcrop.

4.1.2.1. D_1: Top-To-The SE Thrusting

D_1 top-to-the SE thrusting is well documented by S-C tectonites with NE-SW striking and steeply NW dipping (70–85°) S planes and NE-SW striking, and moderately NW dipping (30–70°) C planes decorated by calcite slickenfibers constraining a thrust-related top-to-the SE sense of shear (Figure 6b). These tectonites are only

Table 1
Summary of Sampled Material

	Sample ID	Structural station	Figure	Type	Related kinematics	Host rock	Age of host rock	Structural position	Laboratory analysis	Geochronological result
Valsugana Thrust	VT6	1	Figure 5c	Clay gouge	Top-to-the SE	Metamorphic basement	upper Paleozoic	VT hanging wall	XRD and K-Ar dating	IAA K-Ar age 77.9 ± 15.1 Ma
	VT4	2	Figure 6c	Clay gouge	Top-to-the SE	Dolomia Principale Fm.	Upper Triassic	VT footwall	XRD and K-Ar dating	IAA K-Ar age 128.7 ± 15.3 Ma
	VT10	3	Figure 7c	Clay gouge	Top-to-the SE	Metamorphic basement	upper Paleozoic	VT hanging wall	XRD and K-Ar dating	K-Ar age 76.2 ± 1.4 Ma
	VT9	3	Figure 7d	Fault breccia with calcite cement	Top-to-the SE	Limestone of Calcari Grigi Group	Lower-Middle Jurassic	VT footwall	Petrography and U-Pb dating	U-Pb age 23.2 ± 2.1 Ma
	VT3B	3	Figure 7g	Calcite slickenfiber	Top-to-the SE	Cherty limestone of Maiolica Fm.	Upper Jurassic-Lower Cretaceous	VT footwall	Petrography and U-Pb dating	U-Pb age 15 ± 11 Ma
	VT104	4	Figure 8b	Calcite slickenfiber	Top-to-the SE	Limestone of Calcari Grigi Group	Lower-Middle Jurassic	VT PSS plane	Petrography and U-Pb dating	U-Pb age 9.5 ± 0.8 Ma
	VT101	4	Figure 8c	Calcite vein	Top-to-the SE	Limestone of Calcari Grigi Group	Lower-Middle Jurassic	VT footwall	Petrography and U-Pb dating	U-Pb age 6.0 ± 1.7 Ma
	VT100	4	Figure 8e	Calcite slickenfiber	Top-to-the NW	Limestone of Calcari Grigi Group	Lower-Middle Jurassic	VT footwall	Petrography and U-Pb dating	U-Pb age 46 ± 15 Ma
Belluno Thrust System	BT2	5	Figure 9c	Calcite slickenfiber	Top-to-the SSE	Cherty limestone of Maiolica Fm.	Upper Jurassic-Lower Cretaceous	BT footwall	Petrography and U-Pb dating	U-Pb age 23 ± 14 Ma
	BT1	6	Figure 9d	Clay gouge	Top-to-the SE	Marly limestone of Scaglia Rossa Fm.	Upper Cretaceous-Eocene	SDCT footwall	XRD and K-Ar dating	IAA K-Ar age 29.9 ± 11.2 Ma

Note. VT: Valsugana Thrust; BT: Belluno Thrust; SDCT: San Donato-Costa Thrust. IAA: Illite Age Analysis.

locally preserved (Figure 6a) likely due to the overprinting by the subsequent deformation phases (D_2–D_4). Indeed, D_1 S-C tectonites are systematically cut and displaced by fault planes associated with D_3 (see below; Figures 6a and 6b). A lens of blackish gouge associated with C planes was sampled for XRD analysis and K-Ar dating (sample VT4; Figure 6c).

4.1.2.2. D_2: Top-To-The NW Right-Lateral Transpression

D_2 is represented by one large calcite slickensided fault plane that strikes ENE-WSW and dips moderately to the SSE (40–50°), indicating right-lateral, top-to-the NW transpression (Figures 6a and 6c). A ∼1 m thick and weakly foliated fault core is observed below the very smooth fault surface (Figure 6c). No other structures associated with D_2, hence indicating a transpressional top-to-the NW sense of shear, are observed at the Val Imperina exposure.

4.1.2.3. D_3: Top-To-The NE Right-Lateral Transpression

D_3 is represented by NE-SW-striking and very steeply NW-dipping slickensided fault planes. These are the most abundant deformation structures at the Val Imperina exposure (Figures 6a and 6d–6e) and commonly bear grooves and slickenlines that consistently indicate top-to-the NE right-lateral transpression (Figure 6e). D_3 fault planes systematically cut the S-C tectonites of D_1 (Figures 6a and 6b) and the SSE-dipping fault plane of D_2 (Figures 6a and 6e).

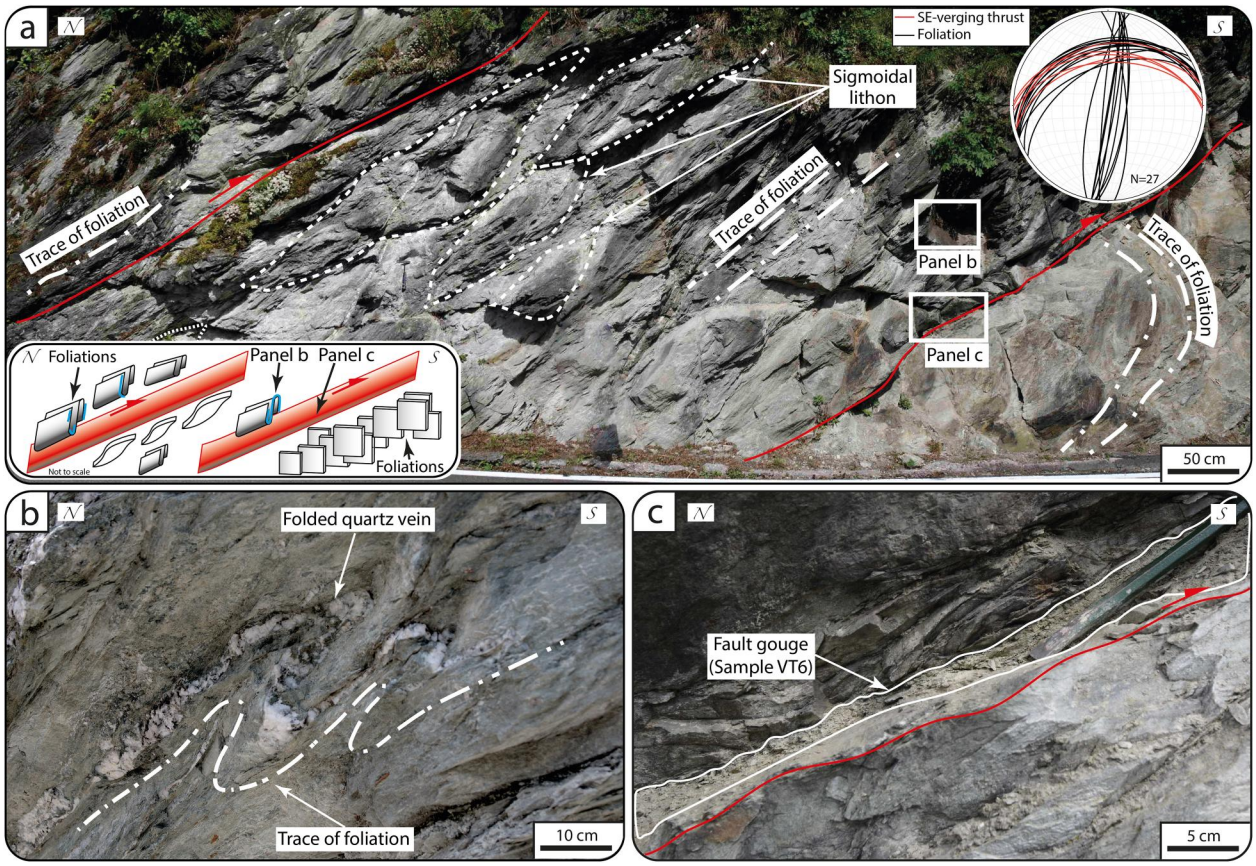

Figure 5. (a) Phyllites of the Paleozoic metamorphic basement deformed by a NNW dipping, SE verging thrust and containing sigmoidal lithons imbricated according to a top-to-the SE sense of shear. Inset in panel (a) shows a schematic representation of the outcrop. (b) Detail of folded quartz vein and foliation. (c) Detail of the thrust surface and related fault gouge lens sampled for K-Ar dating. Lower hemisphere Schmidt net projection of the measured foliations and thrusts is shown in panel (a).

4.1.2.4. D_4: Top-To-The SE Left-Lateral Transpression

NNW-SSE striking and 50–85° WSW-dipping fault planes decorated by calcite slickensides are invariably associated with D_4. They constrain left-lateral top-to-the SE strike-slip to gentle transpression (Figure 6f). These structures systematically cut the NW dipping fault planes of D_3 (Figures 6a–6d and 6f), confirming the D_3 older age. Fault planes associated with D_4 seemingly accommodate a maximum displacement of ∼1 m (Figure 6c).

4.1.3. Structural Station n. 3 (Lat.: 46°07′12″N, Long.: 11°41′23″E; Figure 7)

In locality Passo del Brocon, a NW-SE and ∼3 km long traverse is well exposed, offering unique insights into a large-scale imbricated structure with a general transport toward the SE. The imbricate structure is composed of a sliver of phyllitic metamorphic basement overlying the Lower Jurassic limestone of the Calcari Grigi Group, which, in turn, is thrusted above the Upper Jurassic-Lower Cretaceous pelagic cherty limestone of the Maiolica Fm. The Maiolica Fm. is thrusted above the Upper Cretaceous-lower Eocene marly limestone of the Scaglia Rossa Fm (Figure 7a). The metamorphic basement, whose tectonic contact to the underlying Calcari Grigi Group is exposed along the Forcella della Boia (described in detail below), is deformed by SE verging folds, crenulations and thrusts (Figures 7a and 7b). The thrusts strike NW-SE, dip 15–25° toward the NW and bound metric sigmoidal lithons of less deformed rock (Figures 7a and 7b). Lenses of clay-rich fault gouge locally decorate the thrust in the phyllitic metamorphic basement. We sampled the lenses of fault gouge for K-Ar dating (sample VT10; Figure 7c). Second-order, NW-verging backthrusts are also present within the metamorphic basement and are locally cut by low displacement extensional faults.

The thrust juxtaposing the limestone of the Calcari Grigi Group onto the cherty limestone of the Maiolica Fm. strikes NE-SW, dips 70° to the NW and is decorated by calcite slickenfibers indicating a top-to-the SE sense of

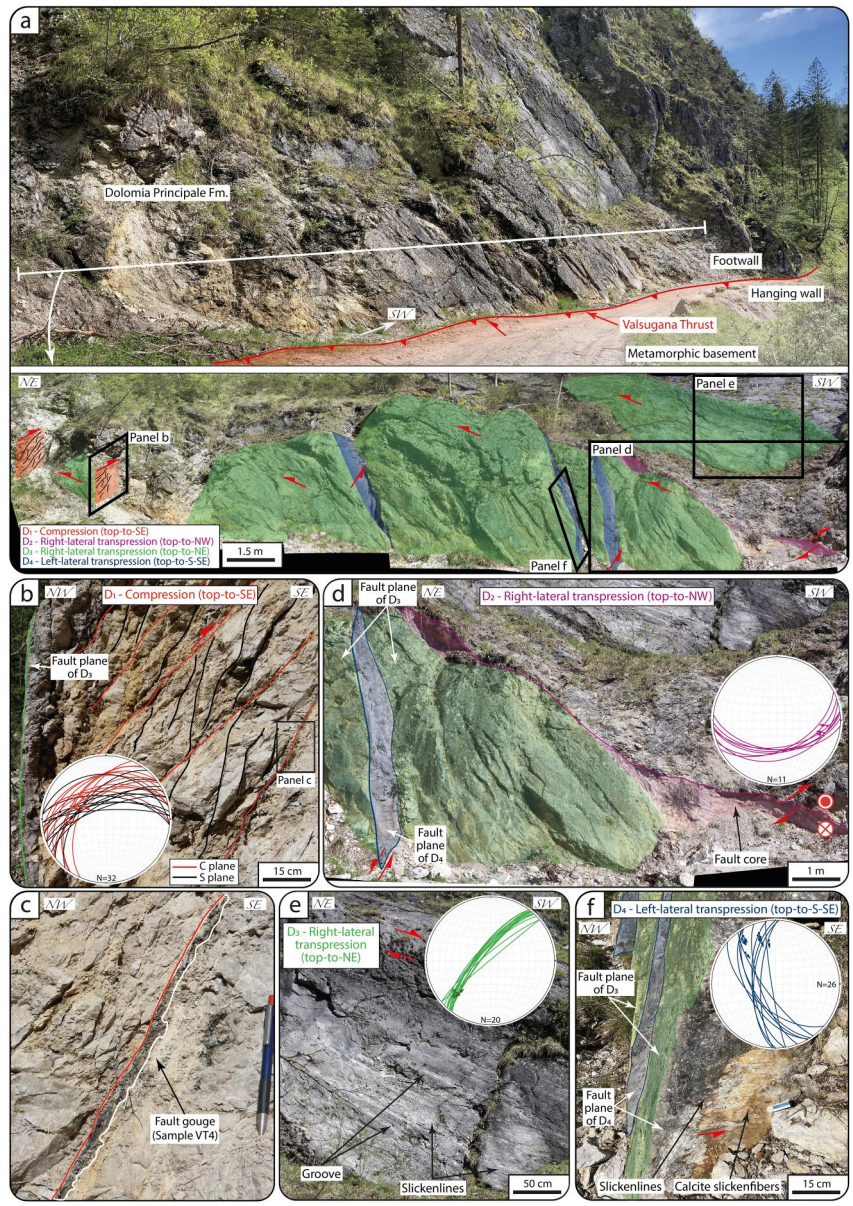

Figure 6. (a) Panoramic view and structural interpretation of the exposure in Val Imperina, where the Valsugana Thrust juxtaposes the metamorphic basement in the hanging wall against the carbonate of the Dolomia Principale Fm., which contains tectonic structures ascribable to four distinct deformation phases (D_1-D_4). (b) Detail of tectonic structures associated with D_1 consisting of top-to-the SE S-C tectonites. A fault plane of D_3 truncating the S-C tectonites is shown. (c) Detail of a blackish gouge lens smeared along a C plane and sampled for K-Ar dating. (d) SSE-dipping fault plane with slickenfibers indicating right-lateral top-to-the NW transpression (D_2). Cutting relationships between structures associated with D_2-D_4 are shown. (e) NW dipping fault plane with grooves, slickenlines, and slickenfibers indicating top-to-the NE right-lateral transpression (D_3). (f) SW dipping slickensided fault plane indicating a top-to-the S-SE sense of shear (D_4). The cutting relationship with D_3 is shown. Lower hemisphere Schmidt net projections of the measured structural features are shown.

movement (Figure 7d). Within the first 5–10 cm above the thrust, the Calcari Grigi Group is brecciated. We collected calcite cement from the breccia for U-Pb dating (sample VT9; Figure 7d). Toward the SE, the limestone is deformed by a second order imbricated structure defined by NE-SW striking, gently SE dipping (5–25°) and NW-verging thrusts bounding sigmoidal lithons (Figure 7a). The tectonic contact between the Maiolica Fm. and Scaglia Rossa Fm. is exposed in the southeasternmost part of the traverse as a NE-SW striking and 20–30° NW dipping thrust decorated by top-to-the SE calcite slickensides (Figures 7a and 7e). Micropaleontological field observations indicate an overturned polarity for the Scaglia Rossa Fm., which crops out with a sub-horizonal

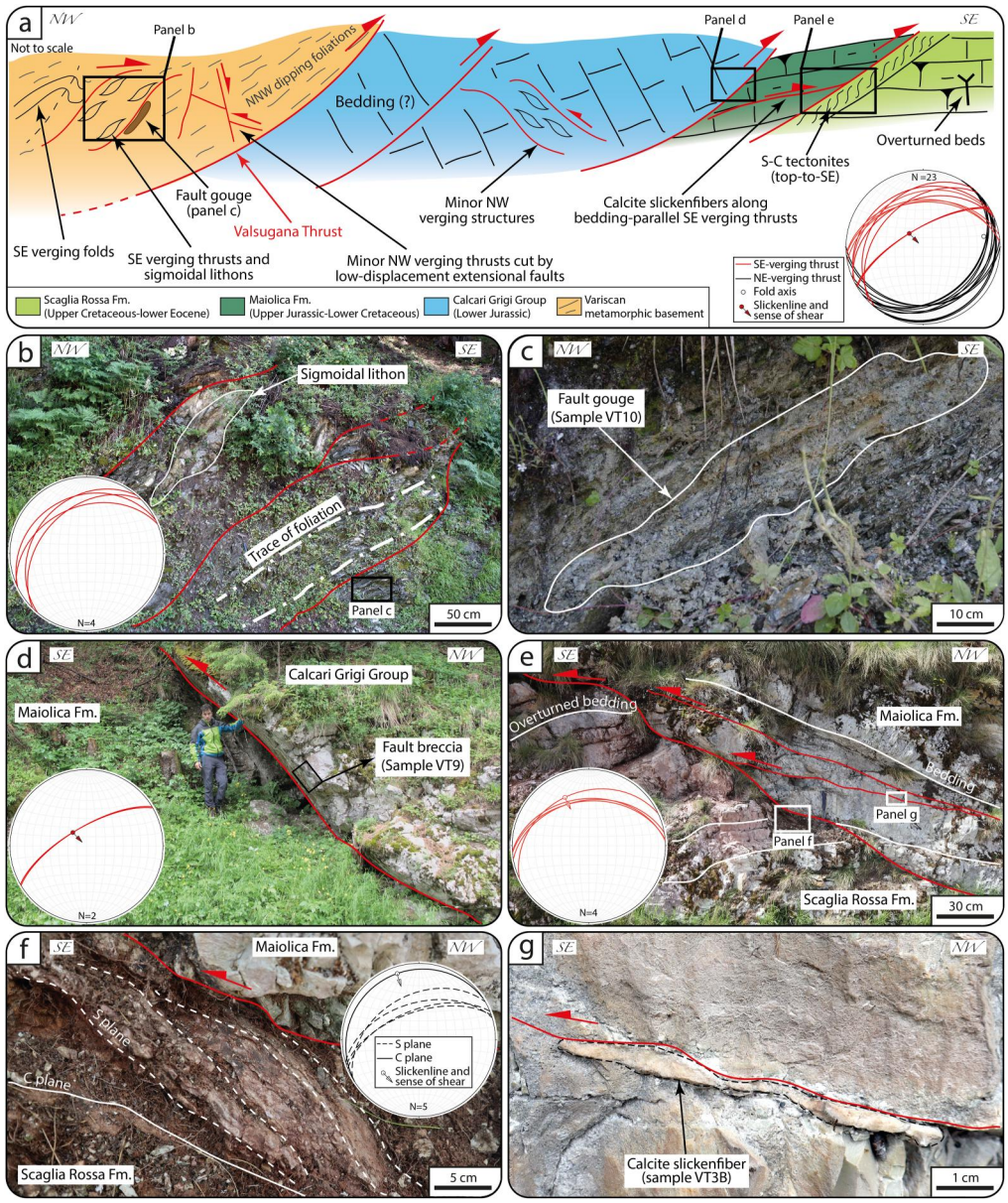

Figure 7. (a) Schematic representation of the ~3 km long section along the Passo del Brocon, where a thrust sheet stack constraining top-to-the SE transport is visible. There, the Valsugana Thrust brought the metamorphic basement toward SE onto the carbonate of the Calcari Grigi Group, in turn thrusted above the marly limestone of the Maiolica Fm., which, in turn, is juxtaposed onto overturned strata of marly limestone of the Scaglia Rossa Fm. (b) NW dipping, SE verging thrusts and sigmoidal lithons within the metamorphic basement. (c) Detail of a sampled lens of fault gouge for K-Ar dating within the metamorphic basement and along a thrust. (d) NW dipping, SE verging thrust juxtaposing the limestone of the Calcari Grigi Group onto the marly limestone of the Maiolica Fm. and site of sampling of fault breccia along the thrust for U-Pb dating. (e) Thrust juxtaposing the limestone of the Maiolica Fm. onto the overturned marly limestone of the Scaglia Rossa Fm. Secondary thrusts within the Maiolica Fm. are also shown. (f) Detail of the Scaglia Rossa Fm. within the first 15 cm below the thrust and showing top-to-SE S-C tectonites. (g) Detail of a calcite slickenfiber occurring along a thrust within the Maiolica Fm. and sampled for U-Pb dating. Lower hemisphere Schmidt net projections of the measured structural features are shown.

bedding deformed by S-C tectonites in the first 10 cm below the thrust (Figures 7a, 7e, and 7f). S planes strike NE-SW and dip 35–60° to the NW. C planes strike NE-SW, dip 5–10° to the NW and contain top-to-SE calcite slickenfibers (Figure 7f). Above the thrust, the Maiolica Fm. dips gently to the NW (Figure 7e) and is deformed by

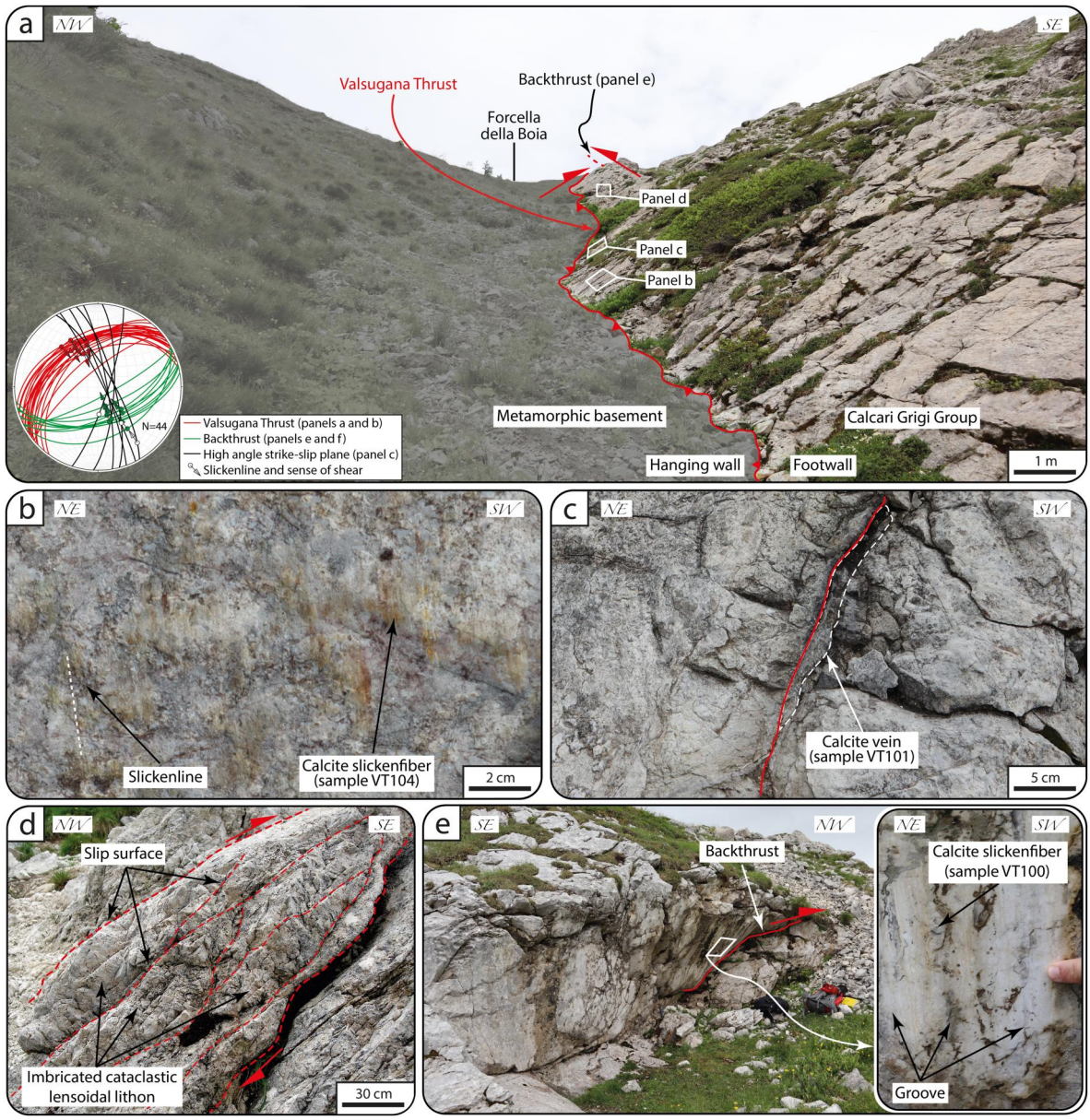

Figure 8. (a) Valsugana Thrust (VT) exposed along Forcella della Boia, where the metamorphic basement is thrusted to the SE onto the carbonate of the Calcari Grigi Group. (b) Detail of the VT with calcite slickenfibers indicating a top-to-the SE sense of shear and site of sampling for U-Pb dating. (c) NW-SE striking strike-slip fault plane bearing a calcite vein that was sampled for U-Pb dating. (d) Cataclastic carbonate leonsoidal lithons in the first meters below the VT with an imbrication toward the SE. (e) SE dipping and NW verging backthrust within the carbonate of the Calcari Grigi Group and detail of the backthrust plane characterized by grooves and calcite slickenfibers sampled for U-Pb dating. Lower hemisphere Schmidt net projection of the measured structural features is shown in panel (a).

NE-SW striking, NW dipping (20–25°) and SE verging thrusts decorated by calcite slickenfibers that we sampled for U-Pb carbonate dating (sample VT3B; Figures 7a, 7e, and 7g).

4.1.4. Structural Station n. 4 (Lat.: 46°07′37″N, Long.: 11°39′56″E; Figure 8)

The VT is directly exposed at Forcella della Boia, ~2 km to the west of structural station n. 3 at Passo del Brocon. There, the thrust juxtaposes the Paleozoic metamorphic basement in the hanging wall to the NW against the carbonate of the Calcari Grigi Group in the footwall to the SE (Figure 8a). The VT principal slip surface (PSS) is locally preserved as dipping 40–50° toward the NW (dip direction: 320–345°) and locally decorated by top-to-the SE striated calcite slickensides (Figures 8a and 8b). We sampled the slickensides for carbonate U-Pb dating

(sample VT104; Figure 8b). High angle (70–90°) NW-SE striking and both NE and SW dipping planes with striae indicating dominant strike-slip movement are observed and are commonly associated with up to 2 cm thick calcite veins sampled for U-Pb dating (sample VT101; Figures 8a and 8c). The Calcari Grigi Group carbonate contains cataclastic lensoidal lithons imbricated to form a top-to-the SE geometry and is bounded by NE-SW striking and NW dipping slip surfaces (Figure 8d). Within it, there occurs a NE-SW striking backthrust with a flat-ramp geometry dipping 40–80° to the SE, which is characterized by a PSS decorated by grooves, striae, and calcite slickenfibers invariably indicating a top-to-the NW sense of shear. We sampled it for U-Pb dating (sample VT100; Figures 8a and 8e).

4.2. Mesostructural Observations and Sampling Along the Belluno Thrust System

4.2.1. Structural Station n. 5 (Lat.: 46°04′34″N, Long.: 11°45′33″E; Figure 9)

At this locality, the limestone of the Maiolica Fm. ~20 m below the BT (Figure 9a) is deformed by closely spaced thrusts that mainly localize along bed-bed interfaces and locally form duplex structures (Figure 9b). Thrusts strike c. E-W, dip 65-20° to the N (Figure 9a) and contain slickenlines and up to 1 cm thick calcite slickenfibers invariably indicating an overall top-to-the S sense of shear (Figures 9b and 9c). We sampled the calcite slickenfibers for microtextural analysis and U-Pb dating (sample BT2; Figure 9c).

4.2.2. Structural Station n. 6 (Lat.: 46°03′13″N, Long.: 11°44′25″E; Figure 9)

In the SDCT footwall, ~2.5 km to the south of structural station n. 5, marly limestones of the Scaglia Rossa Fm. are deformed by a fold train with NE-SW fold axes and NE-SW striking and NW and SE dipping limbs (Figures 9a and 9d). Along the forelimbs and between the beds of marl and marly limestone, discrete lenses of gouge are exposed and have sampled for K-Ar dating (sample BT1; Figure 9d). Folds are cut by NE-SW striking and NW dipping, low displacement (up to 50 cm) top-to-the SSE thrusts (Figure 9d).

4.3. Microtextures of Tectonic Carbonates

The sampled tectonic carbonates are characterized by blocky textures with equidimensional and randomly oriented twinned crystals. In detail, sample VT9 consists of a fault breccia with millimetric to centimetric clasts and fragments of host rock embedded within calcite cement exhibiting a blocky texture (Figure 10a). Samples VT3B and VT104 are fragments of calcite slickenfibers made up of blocky crystals up to ~400 μm in size (Figures 10b and 10c). Sample VT101 is a calcite vein made up of blocky crystals (Figure 10d). Samples VT100 and BT2 consist of calcite slickenfibers made up of blocky crystals up to ~400 μm in size (Figures 10e and 10f).

4.4. X-Ray Diffraction of Clay Gouge

We collected and analyzed three samples of clay gouge formed at the expense of Variscan basement rocks along the VT (samples VT4, VT6, and VT10) and one clay gouge formed at the expense of sedimentary rocks along the BT (BT1; Figure 4 and Table 1). Four size fractions were separated for VT4 and VT6 (from 10 to 0.4–0.1 μm), whereas five fractions were successfully separated for VT10 and BT1 (from 10 to <0.1 μm; Table 2). A total of 18 fractions were thus analyzed for illite-muscovite polytypism and X-ray semiquantitative analysis (Table 1). This allowed us to discriminate between authigenic/syn-kinematic illite ($1M_d$ or 1M polytype) likely formed during faulting and detrital illite/muscovite crystals ($2M_1$ polytype) inherited from the host rock (Figure 11).

Sample VT10 exhibits a slight increase of illite/muscovite-$2M_1$ and chlorite content from the coarsest to finest grain size fraction from 68% to 72% and from 23% to 28%, respectively (Table 2), accompanied by a progressive decrease of paragonite (from 9% in the 2–6 μm to 3% in the 0.4–0.2 μm fraction; Figure S1 in Supporting Information S1) that disappears in the 0.1–0.4 μm and <0.1 μm fractions. Quartz content is 2% in most of the grain-size fractions and absent in the <0.1 μm fraction. Albite only occurs in the coarse fractions, never exceeding 1%.

The mineralogical assemblage of gouge VT6 in the 2–6 and 6–10 μm grain size fractions is mainly defined by quartz, illite/muscovite-$2M_1$ and chlorite, whose contents vary between 91% and 95% of the overall composition. K-feldspar (<2%), calcite (2%) and rutile (2%) as well as traces of dawsonite have also been detected in these fractions. Illite-1 M amounts to 3% in the 2–6 μm grain size fraction. Quartz and chlorite become progressively less abundant in the finer fractions (0.1–0.4 μm, 0.4–2 μm) where a general increase of illite-1M is instead observed from 10% to 28%.

10.1029/2023TC008013

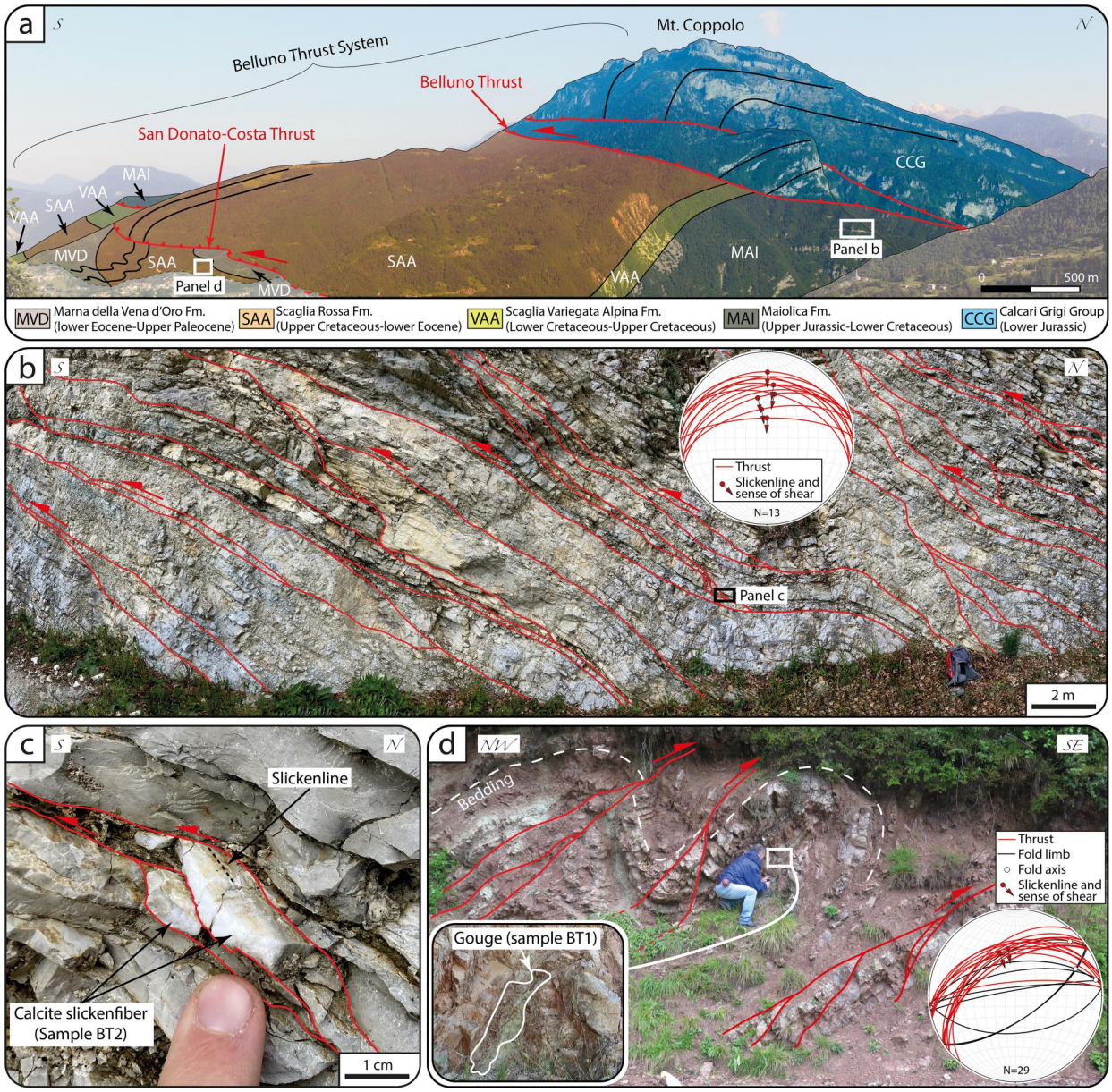

Figure 9. (a) Panoramic view of the Belluno Thrust (BT) System containing the Belluno and San Donato-Costa thrusts. (b) Limestone of the Maiolica Fm. (c) 20 m below the BT and deformed by thrusts mainly localizing along bed-bed interfaces and locally forming duplex structures. (c) Detail of a calcite slickenfiber observed along a thrust plane, constraining a top-to-SSW sense of shear, and sampled for U-Pb dating. (d) Marly limestone of the Scaglia Rossa Fm. located (c) 20 m down into the San Donato-Costa Thrust footwall and deformed by a SE-verging fold train cut by SE verging discrete thrusts. The site of sampling of a fault gouge lense along a fold limb is also shown. Lower hemisphere Schmidt net projections of the measured structural features are shown.

Sample VT4 contains chlorite (30%–32%), dolomite (23%–28%), calcite (11%–12%), illite/muscovite-2M$_1$ (13%–20%) and subordinate paragonite (5%–6%; Figure S1 in Supporting Information S1), quartz (7%) and rutile (3%) in the 2–6 and 6–10 μm grain size fractions. In the 0.4–2 μm fraction we observe the same mineral assemblage as in the coarse fraction except for the neoformation of illite-1M and the absence of calcite (Table 2). Sheet silicates (chlorite, illite-1M and illite/muscovite-2M$_1$) are the dominant clay minerals in the 0.1–0.4 μm fraction forming 94% of the whole-rock mineralogical assemblage.

Gouge BT1, formed at the expense of the Scaglia Rossa Fm., is mainly composed of quartz, calcite and mixed layer illite-smectite (I-S) with contents >94% in the coarse sub-fractions (2–6 μm and 6–10 μm), and by subordinate contents of K-feldspar (1%), albite (1%) and illite/muscovite-2M$_1$ and illite-1M$_d$ polytypes (4%). In the

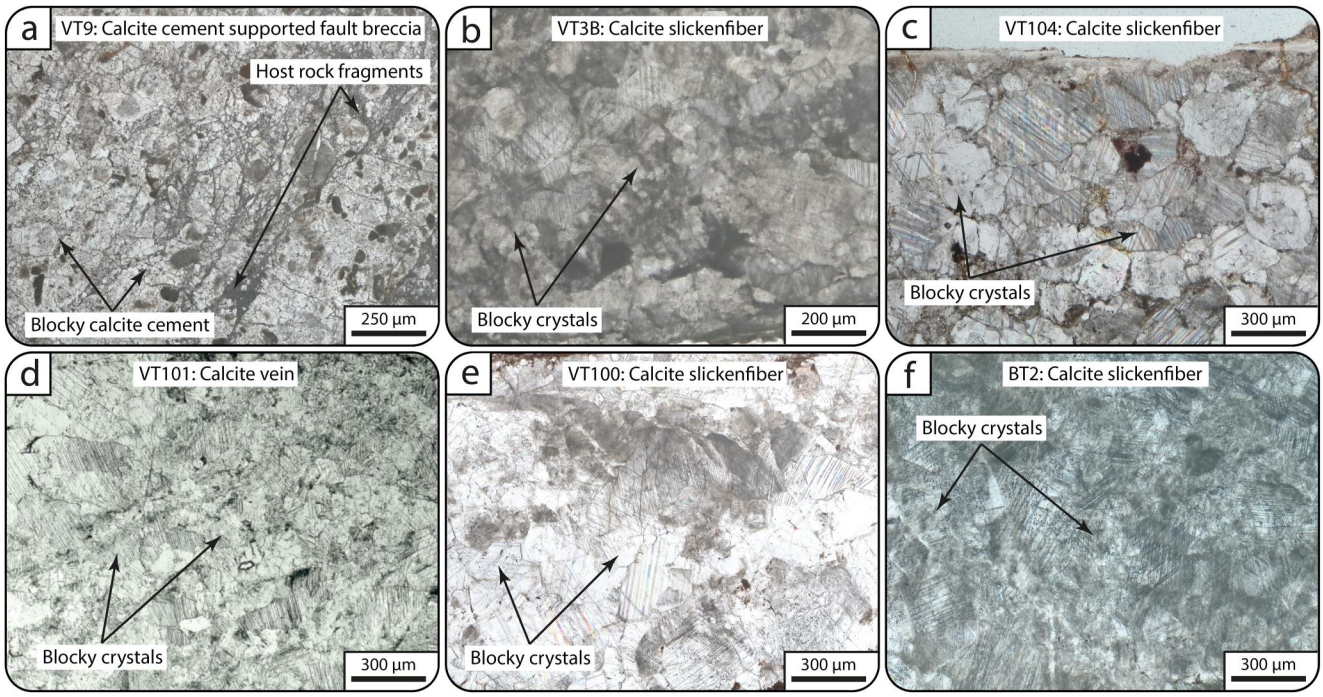

Figure 10. Microstructures of the six dated tectonic carbonates. (a) Sample VT9. Fault breccia with calcite cement made up of blocky crystals. (b) Sample VT3 consisting of a calcite slickenfiber made up of blocky crystals. (c) Sample VT104. Calcite slickenfiber made up of blocky crystals. (d) Sample VT101. Blocky calcite vein. (e) Sample VT100. Calcite slickenfiber with blocky crystals. (f) Sample BT2 consisting of a calcite slickenfiber with blocky crystals.

finer fractions, mixed layer I-S is the dominant clay mineral followed by low amounts of illite-1M (5%–7%) and illite/muscovite-2M$_1$ (2%).

4.5. K-Ar Ages of syn-Kinematic Clay Minerals in Clay Gouge

The 18 grain size fractions separated from clay gouge samples VT4, VT6, VT10, and BT1 have been analyzed by K-Ar isotopic dating (Table 3). For all samples, ages define an inclined spectrum (*sensu* Pevear, 1999; Torgersen et al., 2015) wherein the coarsest fraction yields the oldest age and the finest fraction the youngest age (Figure 12a). From the coarsest to the finest fractions, sample VT4 yields K-Ar ages between 265.3 ± 4.6 Ma (Permian) and 188 ± 3.2 Ma (Early Jurassic), sample VT6 between 274.8 ± 4.5 Ma (Permian) and 164.2 ± 2.8 Ma (Middle Jurassic), sample VT10 between 240.2 ± 3.7 Ma (Middle Triassic) and 76.2 ± 1.4 Ma (Late Cretaceous), and sample BT1 between 168.5 ± 2.5 Ma (Middle Jurassic) and 92.6 ± 1.3 Ma (early Late Cretaceous; Figures 12a and Table 2). The XRD analysis of the fractions of VT4 and VT6 indicates a mixture of detrital illite/muscovite-2M$_1$ and authigenic/syn-kinematic illite-1M, with the latter increasing toward the finest fractions (Figures 12a and Table 2). Thus, the K-Ar ages of the finest fractions represent spurious ages arising from the mixing of different amounts of detrital muscovite 2M$_1$ and authigenic/syn-kinematic illite-1M. Similarly, the K-Ar ages of all the fractions of BT1 are older than the stratigraphic age of the host rock (late Upper Cretaceous-lower Eocene; Figure 12a), suggesting mixing between authigenic/syn-kinematic illite-1M$_d$ and detrital illite-2M$_1$ inherited from the host rock (Figure 12a).

To overcome this issue and obtain geologically meaningful ages, we assessed the effect of contamination of detrital illite/muscovite-2M$_1$ in samples VT4, VT6 and BT1 by the Illite Age Analysis method approach (IAA; Pevear, 1999). In detail, to estimate the age of the authigenic/syn-kinematic illite-1M (samples VT4, VT6) and illite-1M$_d$ (sample BT1) formed during faulting, we normalized to 100% the proportion of illite/muscovite-2M$_1$ and illite-1M or -1M$_d$ (as determined by XRD analysis; Table 2) plotting the data as apparent K-Ar age versus percentage of detrital illite/muscovite-2M$_1$, and linearly extrapolated to 0% and 100% authigenic illite-1M and -1M$_d$ polytypes by York regression (e.g., York et al., 2004, Figure 12b). By means of this regression, the age of the last deformation event recorded by VT4 is 128.7 ± 15.3 Ma, by VT6 is 77.9 ± 15.1 Ma, and by BT1 is 29.9 ± 11.2 Ma (Figure 12b).

Table 2
Whole-Rock Composition of Various Grain-Size Fractions for Gouges From the Valsugana Thrust (VT4, VT6, and VT10) and Belluno Thrust (BT1)

			Whole-rock composition (% wt)												
Sample ID	Host rock	Grain-size fraction (μm)	Qz	Kfs	Ab	Cal	Dol	Pg	I-2M$_1$	I-1M	I-1M$_d$	I-S	Chl	Rt	Dws
VT4	Dolomia Principale Fm.	0.1–0.4	6	–	–	–	–	–	25	26 16–	–	–	40	–	–
VT4		0.4–2	9	–	–	–	6	3	27		–		37	2	–
VT4		2–6	7	–	–	12	23	5	20		–		30	3	–
VT4		6–10	7	–	–	11	28	6	13		–		32	3	–
VT6	Metamorphic basement	0.1–0.4	8	–	–	–	–	–	20	28	–	–	44	–	tr
VT6		0.4–2	17	1	–	2	–	–	23	10	–	–	47	–	tr
VT6		2–6	18	2	–	2	–	–	22	3	–	–	51	2	tr
VT6		6–10	21	1	–	2	–	–	22	–	–	–	52	2	tr
VT10	Metamorphic basement	<0.1	–	–	–	–	–	–	72	–	–	–	28	–	–
VT10		0.1–0.4	2	–	–	–	–	–	68		–		30	–	–
VT10		0.4–2	2	–	–	–	–	3	70		–		25	–	–
VT10		2–6	2	–	1	–	–	9	67		–		21	–	–
VT10		6–10	2	–	1	–	–	6	68		–		23	–	–
BT1	Marly limestone of the Scaglia Rossa Fm.	<0.1	6	–	–	–	–	–	2	–	7	85	–	–	–
BT1		0.1–0.4	11	–	1	14	–	–	2		5	67	–	–	–
BT1		0.4–2	16	1	1	35	–	–	2		3	42	–	–	–
BT1		2–6	15	1	1	58	–	–	2		2	21	–	–	–
BT1		6–10	12	1	1	63	–	–	2		2	19	–	–	–

Note. *Qz*, Quartz; Kfs: K-feldspar; *Ab*, Albite; *Cal*, Calcite; *Dol*, Dolomite; *Pg*, Paragonite; *I-2M$_1$*, Illite-muscovite-2M$_1$; *I-1M*, Illite-1M; *I-1M$_d$*, Illite-1M$_d$; *I-S*, Mixed layer illite-smectite; *Chl*, Chlorite; *Rt*, Rutile, *Dws*, Dawsonite; *tr*, Trace (<1%).

4.6. U-Pb Ages of Tectonic Carbonates

Out of >30 collected samples from the area, we obtained U-Pb dates on only five tectonic carbonates from along the VT (samples VT9, VT3B, VT100, VT101, and VT104) and one tectonic carbonate from along the BT (sample BT2; Figure 3 and Table 1). The unsuccessful samples were characterized by low U contents. The dated samples yielded analytically reliable dates that are 23.2 ± 2.1 Ma (MSWD = 2.8; n = 37 of 49) for sample VT9, 15 ± 11 (MSWD = 0.43; n = 60 of 60) Ma for sample VT3B, 9.5 ± 0.8 Ma (MSWD = 3.8; n = 78 of 104) for sample VT104, 6.0 ± 1.7 Ma (MSWD = 5.9; n = 112 of 134) for sample VT101, 46 ± 15 Ma (MSWD = 8; n = 135 of 135) for sample VT100, and 23 ± 14 Ma (MSWD = 0.76; n = 130 of 130) for sample BT2 (Figure 13 and Table S1 in Supporting Information S2).

Some of these ages yielded large uncertainties (because of low radiogenic/common Pb values); nevertheless, the data as a whole provide for significant improvement in constraining the timing of faulting in the study area. For the samples with higher precision (VT100, VT101, VT104, and VT9), upper intercepts were more radiogenic, implying that fluids that formed calcite were both higher in U, and radiogenic Pb. We suspect some of the high MSWDs in those samples are from fluids with slightly variable but generally more radiogenic common Pb values than typical common Pb for rocks of that age. In fact, less radiogenic values for sample VT9, tended to have higher initial $^{207}Pb/^{206}Pb$ values, possibly suggesting that those were inclusions or reflect a possible open system behavior with less radiogenic initial Pb.

5. Discussion

5.1. Geometric and Kinematic Constraints

Structural data from the VT and BTS document a remarkable structural complexity. As observed at Passo del Brocon (structural station n. 3; Figures 4 and 7), the sedimentary cover is locally overturned suggesting that it

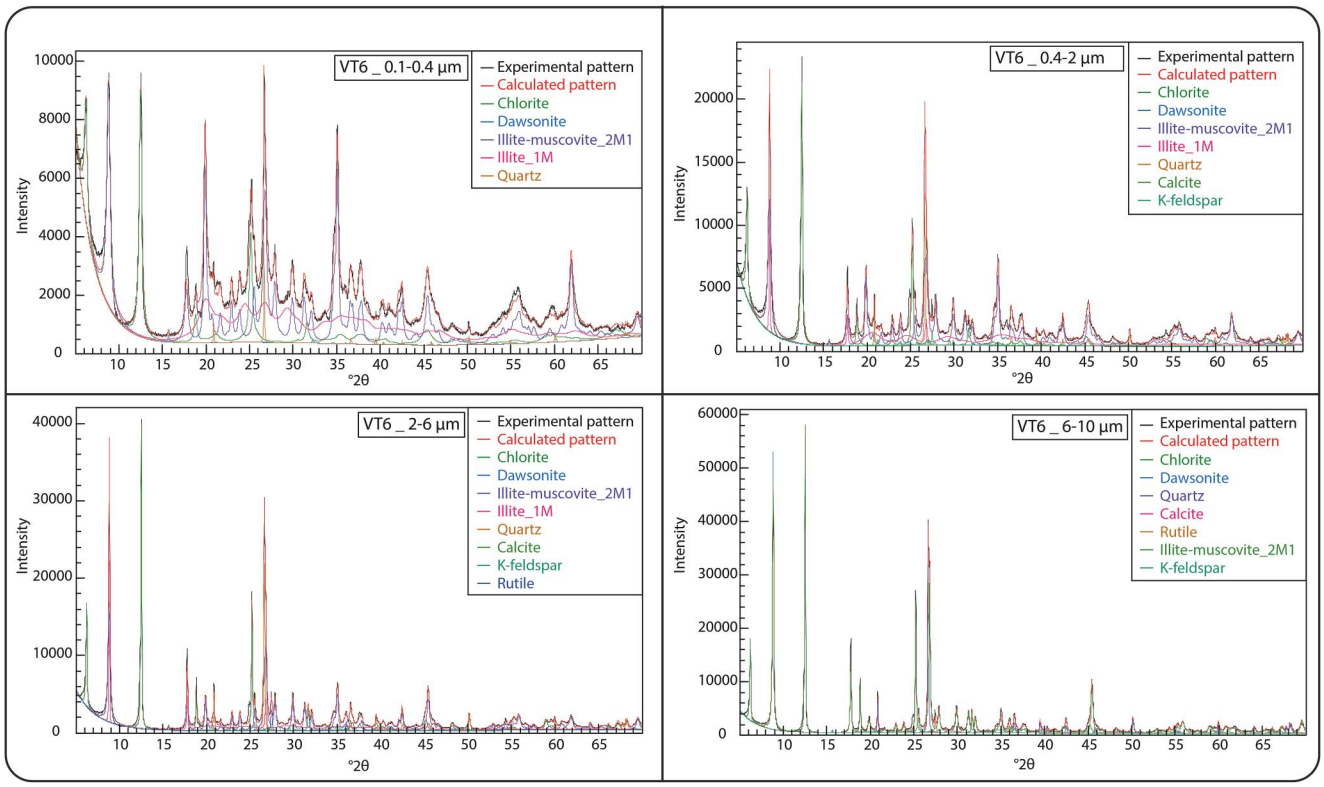

Figure 11. Selected X-ray diffraction patterns of randomly oriented mounts for the different grain-size fractions and polytype characterization of sample VT6. The estimated error on phase quantification is ±1%.

Table 3
K- Ar Data for the Gouge Samples of the VT and BT

		K		^{40}Ar*			Age data	
Sample ID	Grain-size fraction (µm)	wt %	σ (%)	mol/g	σ (%)	^{40}Ar* %	Age (Ma)	σ (Ma)
VT4	0.1–0.4	3.96	1.7	1.359 E+05	0.5	85.9	188	3.2
VT4	0.4–2	4.42	1.7	1.954 E+05	0.6	91.4	238.4	4
VT4	2–6	3.70	1.8	1.781 E+05	0.5	93.5	258	4.4
VT4	6–10	3.54	1.8	1.754 E+05	0.5	94.3	265.3	4.6
VT6	0.1–0.4	3.95	1.7	1.176 E+05	0.5	91.2	164.2	2.8
VT6	0.4–2	4.02	1.7	1.621 E+05	0.5	92.3	218.6	3.7
VT6	2–6	4.09	1.7	1.984 E+05	0.5	96.3	260.1	4.4
VT6	6–10	4.12	1.7	2.119 E+05	0.5	89	274.8	4.5
VT10	<0.1	3.61	1.8	4.869 E+04	0.5	80.8	76.2	1.4
VT10	0.1–0.4	4.45	1.7	9.540 E+04	0.5	90.8	119.5	2
VT10	0.4–2	5.04	1.6	1.745 E+05	0.5	96.3	189.5	3
VT10	2–6	5.31	1.5	2.220 E+05	0.5	97.9	226.1	3.5
VT10	6–10	5.34	1.6	2.380 E+05	0.5	98.5	240.2	3.7
BT1	<0.1	2.56	1.4	4.209 E+04	0.3	41.9	92.6	1.3
BT1	0.1–0.4	2.51	1.4	5.146 E+04	0.3	58.4	114.3	1.6
BT1	0.4–2	2.21	1.5	5.931 E+04	0.3	74.8	148.3	2.1
BT1	2–6	1.55	1.5	4.897 E+03	0.3	83.5	173.3	2.5
BT1	6–10	1.37	1.5	4.184 E+03	0.3	81.4	168.5	2.5

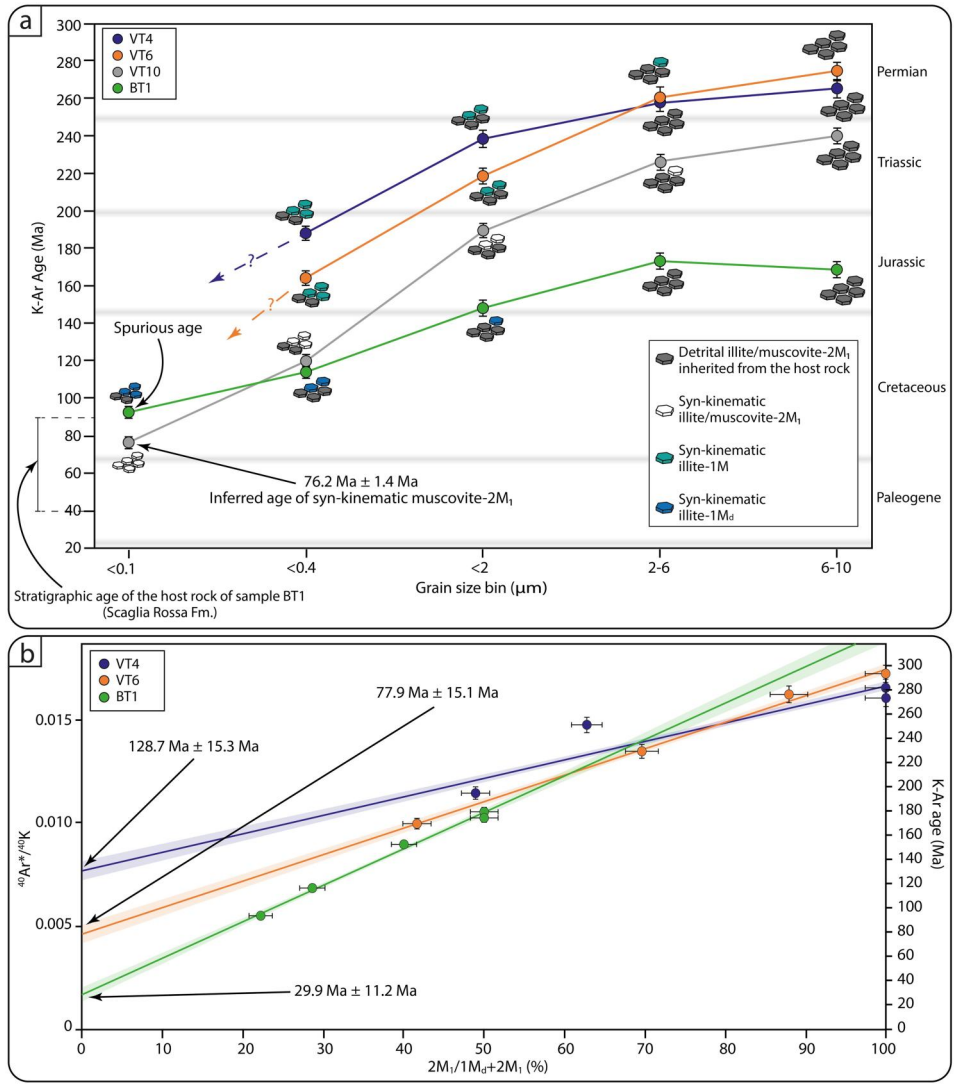

Figure 12. (a) K-Ar age versus grain size. Dark gray horizontal bars broadly define geological time intervals. Notice the inclined age versus grain size curves. The micelle of illite and muscovite polytypes defined by XRD analysis are shown. The depositional age of the host rock of sample BT1 is shown. (b) York regression (colored lines) and error envelop (colored shadows) of Illite Age Analysis (IAA) for the clay gouges for samples VL4, VL6, and BT1. To estimate the age of the authigenic/syn-kinematic illite-1M (samples VL4 and VL6) and illite-1Md (sample BT1), which corresponds to the last deformation event recorded by clay gouge samples, K-Ar ages versus percentage of illite/muscovite-2M_1 (normalized to 100%) are plotted and linearly extrapolated to 0% muscovite-2M_1 and illite-2M_1. The age of the regressed authigenic/syn-kinematic illite-1M recorded by samples VL4 and VL6 and illite-1Md recorded by sample BT1 are shown.

accommodated significant shortening leading to fault-propagation folding causing overturned NE-SW striking folds (with gently NW-dipping overturned forelimbs), before the SE-ward overthrtusting of metamorphic basement onto the folded sedimentary cover and progressive SE-ward stacking took place (Figure 7a). A similar structural architecture, with inclined folds cut by later discrete thrusts, has been observed (Figures 9a and 9d) and recently documented along the BTS (Zuccari et al., 2022).

Kinematic data indicate a dominant and diffuse top-to-the SE transport during shortening and stacking within the studied portion of the ESA. Conjugate top-to-the NW thrusts (Figures 6d, 7a and 8a and 8e) and, to a lesser extent, strike-slip faults (Figures 8a and 8c) have also been recognized as kinematically and mechanically compatible with the SE-ward thrusting along the VT. All these features are consistent with overall NW-SE compression accommodated by shortening along the VT and Venetian Pre-Alps during the Alpine orogenesis (e.g., Castellarin & Cantelli, 2000; Castellarin et al., 2006; Doglioni, 1992; Doglioni & Carminati, 2008). However, a few

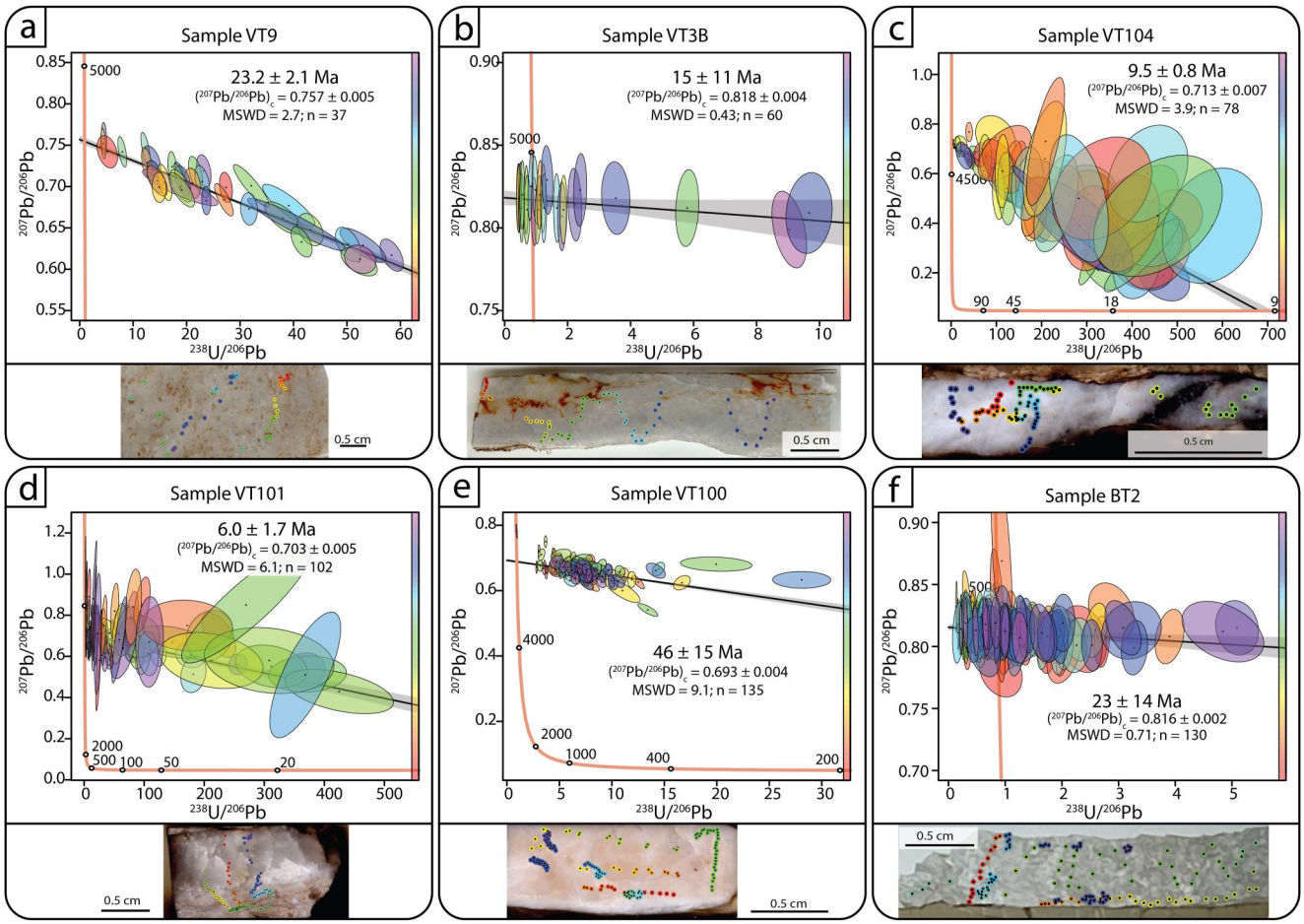

Figure 13. U-Pb Tera-Wasserburg plots and spot location for the dated tectonic carbonates. Color-coding allows to track each analysis between the TW plots and mounts. MSWD: mean square weighted deviation. (a) Calcite cement in fault breccia within limestone of Calcari Grigi Group along the Valsugana Thrust (VT) (structural station n. 3). (b) Calcite slickenfiber within marly limestone of maiolica Fm. along the VT (structural station n. 3). (c) Calcite slickenfiber along the VT principal slip surface (structural station n. 4). (d) Calcite vein within the shallow water carbonate of Calcari Grigi Group along the VT (structural station n. 4). (e) Calcite slickenfiber along a backthrust in the VT footwall and associated with the VT (structural station n. 4). (f) Calcite slickenfibers within pelagic limestone of Maiolica Fm. in the Belluno Thrust footwall (structural station n. 5).

considerations on some local geometric and kinematic peculiarities are necessary. Indeed, meso-structural observations within the Dolomia Principale Fm. along the VT in Val Imperina (structural station n. 2; Figure 4) indicate a relatively late phase of top-to-the NE right-lateral transpression (D_3) and of top-to-the SE left lateral transpression (D_4; Figures 6a–6e and 6f), which may be difficult to reconcile with continued NW-SE compression. In map view, however, structural station n. 2 is located along a ∼1 km long NNE-SSW striking VT oblique ramp (Figure 4) such that it is reasonable to assume that local transpressional movements along this segment of the VT reflect a local component of obliquity.

Furthermore, consistent kinematic indicators along the BTS constrain dominant top-to-the SSE thrusting (Figure 9), that is, slightly oblique to the more common NW-SE shortening direction. As documented from previous studies, however, the BTS is characterized by multiple phases of activation that accommodated tectonic transport along a range of directions, from top-to-the SE to top-to-the SSW (Sieberer et al., 2023; Vignaroli et al., 2020; Zuccari et al., 2021, 2022). The BTS is characterized by a salient to the east (promoted by the involvement of the basinal carbonate multilayer of the Belluno graben) and a recess to the west (affecting the carbonate multilayer of the Trento horst; e.g., Doglioni, 1992; Doglioni & Carminati, 2008, Figure 4). Hence, our kinematic data are coherent with the roughly E-W oriented recess (Figure 4) where the studied segment of the BTS is located and where dominant tectonic transport toward the S/SSE has consistently been reported (e.g., Vignaroli et al., 2020; Zuccari et al., 2021, 2022).

5.2. K-Ar and U-Pb Absolute Time Constraints

5.2.1. The Valsugana Thrust

The grain size-K-Ar age correlation for samples VT4 and VT6 is interpretable as the result of mixing between muscovite-illite $2M_1$ inherited from the host rock (metamorphic basement) and authigenic/syn-kinematic illite 1M. The latter progressively increases in amount toward the finer fractions and is thus interpreted as having formed during the last recorded increment of deformation (e.g., Pevear, 1999, Figure 11a). This agrees with the Age Attractor Model (AAM; Torgersen et al., 2015; Viola et al., 2016), which implies that the amount of detrital K-bearing minerals inherited from the host rock in a fault rock decreases with the decreasing grain size of the dated fractions, whereas the amount of authigenic/syn-kinematic clay increases with decreasing size. Hence, when dealing with K-Ar geochronology of clay gouge it is generally assumed that the finest dated fraction (mostly) consists of syn-kinematic illite as the K-bearing phase (e.g., Torgersen et al., 2015). In samples VT4 and VT6 it was unfortunately not possible to separate the <0.1 μm fraction. This notwithstanding, the IAA approach (Pevear, 1999) allows us to calculate the age of the syn-kinematic illite 1M, which is 128.7 ± 15.3 Ma (Early Cretaceous) and 77.9 ± 15.1 Ma (Late Cretaceous) for VT4 and VT6, respectively. These two dates are thus considered to date the last recorded deformation episode (Figures 12b and 14). Sample VT10 is characterized by an increase of illite/muscovite $2M_1$ from the coarsest to the finest fraction (Figure 12a and Table 2). Hence, considering the typical grain size-K-Ar age correlation (Figure 12a) and the AAM, it is likely that syn-kinematic illite/muscovite $2M_1$ formed in sample VT10. Hence, the 76.2 ± 1.4 Ma (Late Cretaceous) K-Ar age of its finest fraction (Figure 12a) represents the age of syn-kinematic authigenesis. This absolute time constraint is consistent with the Late Cretaceous age (77.9 ± 15.1 Ma) obtained from sample VT6 (Figures 12b and 14).

The tectonic carbonates sampled within the Lower Jurassic-Lower Cretaceous sedimentary cover deformed by the VT (Figure 4) are invariably characterized by blocky textures (Figures 10a–10e) attesting to one single crack-and-seal episode at the sample scale during deformation. Calcite slickenfibers with blocky textures may have formed as a result of fracture opening and fluid filling prior to fault slipping that striated the blocky calcite itself. Hence, the U-Pb ages of the slickenfibers with blocky textures are the oldest possible ages of the tectonic slip along the sampled slickensided surfaces. The obtained U-Pb dates span the early Eocene-Late Miocene time interval and define five tectonic episodes between 46 ± 15 Ma (early Eocene), 23.2 ± 2.1 Ma (late Oligocene), 15 ± 11 Ma (Middle Miocene), 9.5 ± 0.8 Ma (Late Miocene), and 6.0 ± 1.7 Ma (Late Miocene; Figures 13a–13e and 14). These dates are systematically younger than the K-Ar ages from the clay gouges sampled from the Variscan metamorphic basement.

According to previous studies, the VT initially formed by reactivating an early Permian precursor structure during Serravallian-Tortonian times (Figure 14) as indicated by (a) syn-tectonic clastic deposits locally preserved in its footwall (Castellarin et al., 1992; Selli, 1998; Venzo, 1939), (b) apatite fission-track data in the hanging wall indicating exhumation and cooling associated with uplift and erosion between ∼12 Ma and ∼8 Ma (Dunkl et al., 1996), and (c) crosscutting relationships between the VT and NW-SE striking thrusts of Paleogene age (Dinaric phase) in the easternmost portion of the ESA (Carnic Alps; Castellarin & Cantelli, 2000, Figure 2a). Zattin et al. (2003, 2006) and Heberer et al. (2017) applied apatite fission-track and (U-Th-Sm)/He thermochronology to the VT hanging wall constraining (a) very slow exhumation and cooling in the VT hanging wall from ∼77 Ma (Late Cretaceous; Figure 14) and (b) rapid exhumation and cooling associated with the VT activity between ∼12 Ma and ∼8 Ma.

The 128.7 ± 15.3 Ma IAA K-Ar age of sample VT4 (Early Cretaceous) is consistent neither with currently available stratigraphic and fission-track data nor with other geochronological constraints. Also, that age is essentially coeval with the onset of the Alpine Tethys subduction, which is generally constrained to ∼130 Ma (Handy et al., 2010, Figure 14). Hence, while we consider as geologically meaningful the IAA K-Ar age of sample VT4, we discard the 128.7 ± 15.3 Ma date from the tectonic model discussed below.

All other K-Ar and U-Pb dates of our study are consistent with the aforementioned independent geological constraints and document a remarkably long (∼72 Myr) activity for the VT (and its intimately associated structures) from the Late Cretaceous (∼78 Ma) to the Messinian (∼6 Ma; Figure 14). In detail, our K-Ar geochronological data constrain a component of VT faulting to a time between ∼78 Ma and ∼76 Ma (Late Cretaceous), when early orogenic shortening was accommodated by top-to-SE thrusts within the metamorphic basement and by slow exhumation and cooling of the VT hanging wall (Heberer et al., 2017; Zattin et al., 2003,

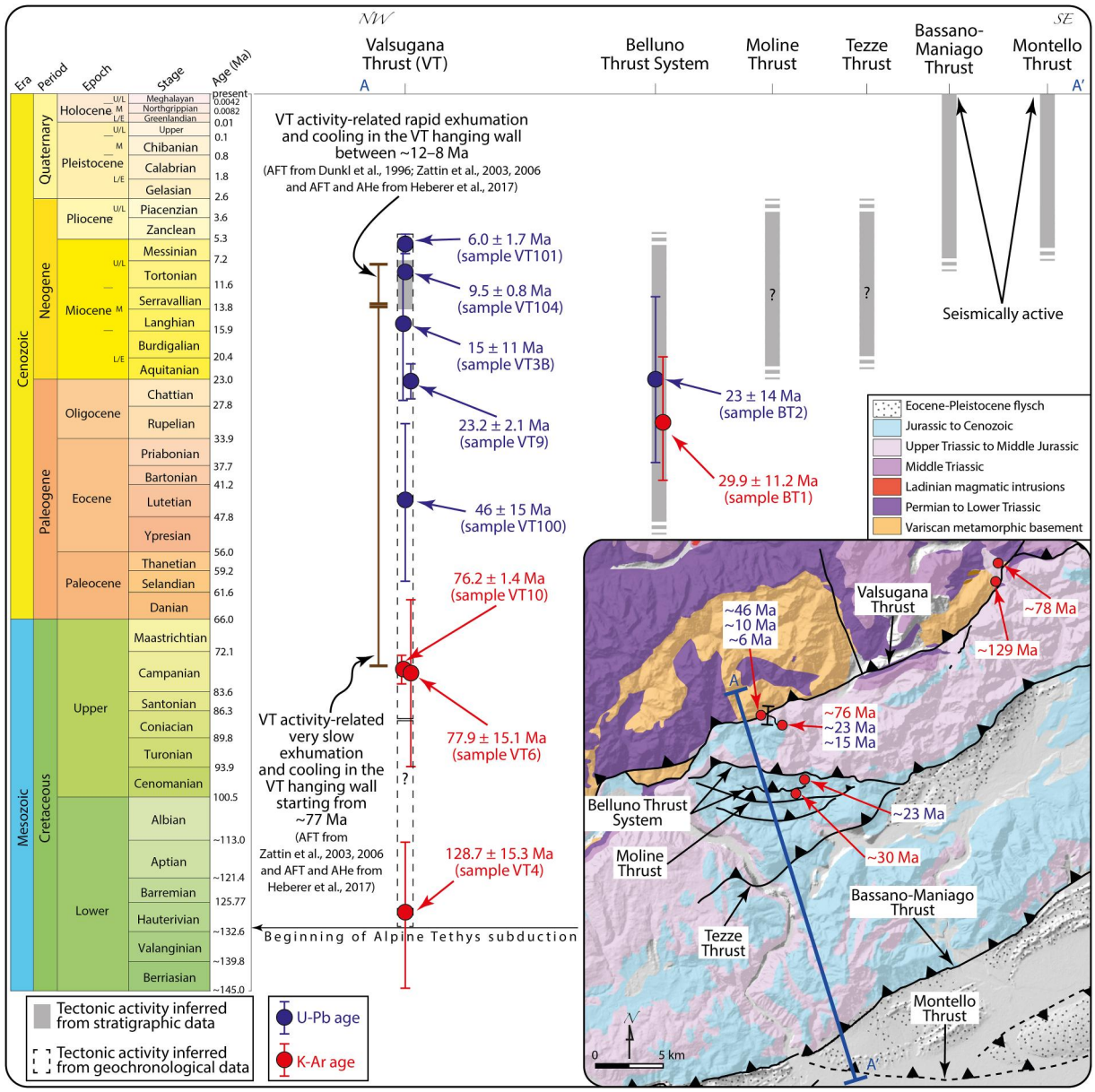

Figure 14. Time-distance diagram for the main regional thrusts of the Eastern Southern Alps (ESA). The trace of the NW-SE time-distance section (A-A′) across the ESA is shown by the blue line. Gray rectangles represent the time of thrust activity as inferred from available time constraints. In detail, stratigraphic data for the Valsugana Thrust (VT) are from Venzo (1939), Selli (1998), Castellarin et al. (1992), Doglioni (1992), and Castellarin and Cantelli (2000). Stratigraphic data for the Belluno Thrust System are from Selli (1998), Doglioni (1987, 1990, 1992), and Castellarin and Cantelli (2000). Stratigraphic and seismic reflection profile data for the Bassano-Maniago and Montello thrusts are from Selli (1998), Caputo et al. (2010), and Picotti et al. (2022). The very slow exhumation and cooling of the VT hanging wall starting from ~77 Ma is constrained by apatite fission track (ATF) data from Zattin et al. (2003, 2006) and ATF and (U-Th-SM)/He (AHe) thermochronology data from Heberer et al. (2017). The rapid exhumation and cooling of the VT hanging wall between ~12 and 8 Ma is from AFT data from Dunkl et al. (1996) and Zattin et al. (2003, 2006) and AFT and AHe data from Heberer et al. (2017). The onset of Alpine Tethys subduction at ~131 Ma is from Handy et al. (2010).

2006). The tectonic activity along the VT continued through time as the thrust progressively propagated toward shallower crustal levels eventually juxtaposing the metamorphic basement atop the Mesozoic cover.

5.2.2. The Belluno Thrust System and Venetian Pre-Alps

The presence of Eocene flysch along the BTS (Figures 2a and 4) suggests the onset of its tectonic activity during Eocene-Oligocene times (Doglioni, 1992). Even though each dated fraction of sample BT1 represents a spurious age due to the mixture of detrital and syn-kinematic K-bearing minerals (Figure 12a), the IAA approach allowed

us to constrain the age of the syn-kinematic component to 29.9 ± 11.2 Ma and to consider it as the age of the last deformation increment recorded by sample BT1. A second absolute time constraint on the BTS is the 23 ± 14 Ma U-Pb age of sample BT2. This date stems from a calcite slickenfiber with a blocky texture (Figure 10f). Considering the error associated with the K-Ar (29.9 ± 11.2 Ma) and U-Pb (23 ± 14 Ma) dates, we can determine a time interval between 41.1 Ma (29.9 Ma +11.2 Ma) and 18.7 Ma (29.9 Ma–11.2 Ma), and between 37 Ma (23 Ma +14 Ma) and 9 Ma (23 Ma–14 Ma), respectively (Figure 14). Based on this, an overlap between 37 Ma (23 Ma +14 Ma) and 18.7 Ma (29.9 Ma–11.2 Ma) is evident, as it is an overall consistency with available stratigraphic time constraints for the BTS activity (Figure 14). By considering our field observations and the structural position of samples BT1 and BT2, a more detailed interpretation of the obtained K-Ar and U-Pb data can be provided. In detail, the ∼30 Ma IAA K-Ar age constrains the time of crystallization of authigenic clays during faulting in the immediate SDCT footwall, which is a splay of the BT (e.g., Zuccari et al., 2021, 2022, Figures 9a and 9d). On this ground, this date may constrain the initiation of BTS-related deformation, when shortening in the sedimentary cover was accommodated by folds and thrusts. The ∼23 Ma U-Pb age constrains, instead, fluid-assisted faulting and related calcite slickenfiber precipitation along a discrete thrust surface associated with the continuing BT activity (Figures 9a–9c). Therefore, the latter age may reflect the timing of a last and discrete localization event along the BTS (i.e., BT and SDCT) and related minor thrusts. This time-constrained scenario is consistent with the observed folds cut by thrusts as repeatedly observed along the BTS (Figure 9d) and discussed in Section 5.1.

Time constraints on the onset of thrusting along the more external (southernmost) and still seismically active thrusts (e.g., Anderlini et al., 2020; Anselmi et al., 2011; Bignami et al., 2012; Cheloni et al., 2014; Galadini et al., 2005; Serpelloni et al., 2016; Viganò et al., 2015) remain indirect and are provided by seismic reflection profiles imaging growth geometries forming at ∼10-9 Ma (Tortonian) and 8-6 Ma (Tortonian-Messinian) in association with the onset of thrusting along the Bassano Maniago Thrust and Montello Thrust, respectively (Picotti et al., 2022, Figure 14). Accurate time constraints on the tectonic activity of Moline and Tezze thrusts, which are located between the BTS and the Bassano-Maniago Thrust, are not available in the literature. According to the overall in-sequence thrust tectonics proposed for the evolution of the Venetian Pre-Alps (Doglioni, 1992), we can only assume that the activity of Moline and Tezze thrusts spans the Oligocene-Pliocene time interval (Figure 14).

5.3. A New Picture for the Long-Term Tectonic Evolution of the Eastern Southern Alps

Our new results call for some reconsideration of the long established and widely acknowledged evolutionary scheme of the ESA by introducing new and hitherto unknown time constraints. This is particularly the case for the K-Ar Cretaceous gouge ages. To provide a possible updated picture of the regional-scale and long-term tectonic evolution of the SA, we compare our geochronological results with available time constraints on the S-verging thrust activity in the cSA.

The new K-Ar Cretaceous ages do not fit the well-known and widely accepted phase of Miocene thrusting in the ESA, the age of which, however, is not based on absolute deformation age constraints (Figure 14; e.g., Doglioni, 1992; Castellarin & Cantelli, 2000). Considering the difference between the new Cretaceous ages and the Miocene timing of thrust activity proposed in the literature, our new results have to be taken with caution and considered conservatively.

In the broader evolutionary picture of the entire SA, however, our Cretaceous ages might acquire a significance. Indeed, the Late Cretaceous VT-related K-Ar ages fit well the ∼80-68 Ma time interval constrained by $^{40}Ar/^{39}Ar$ pseudotachylytes ages from along the OT and PT in the cSA (Zanchetta et al., 2011, Figure 15a). Interestingly, deformation ages from the cSA also fit (a) thermocronological data constraining the exhumation of the basement in the Late Cretaceous (Viola et al., 2001) and (b) the presence of Upper Cretaceous flysch in the cSA (Fantoni et al., 2004).

Our K-Ar Late Cretaceous ages derive from fault gouges formed at the expense of the metamorphic basement (Table 1), which strengthens their reliability and possible geological meaning, even though they predate the classically accepted onset of the VT-related Alpine shortening. This makes it possible to propose an evolutionary tectonic model wherein it is the deeper structural levels to register the first shortening increments. Such a tectonic activity may be interpreted as resulting from far-field stresses potentially affecting the area during the subduction of the Alpine Tethys (Figure 15). Far-field tectonics has been documented as rather common a feature in many

10.1029/2023TC008013

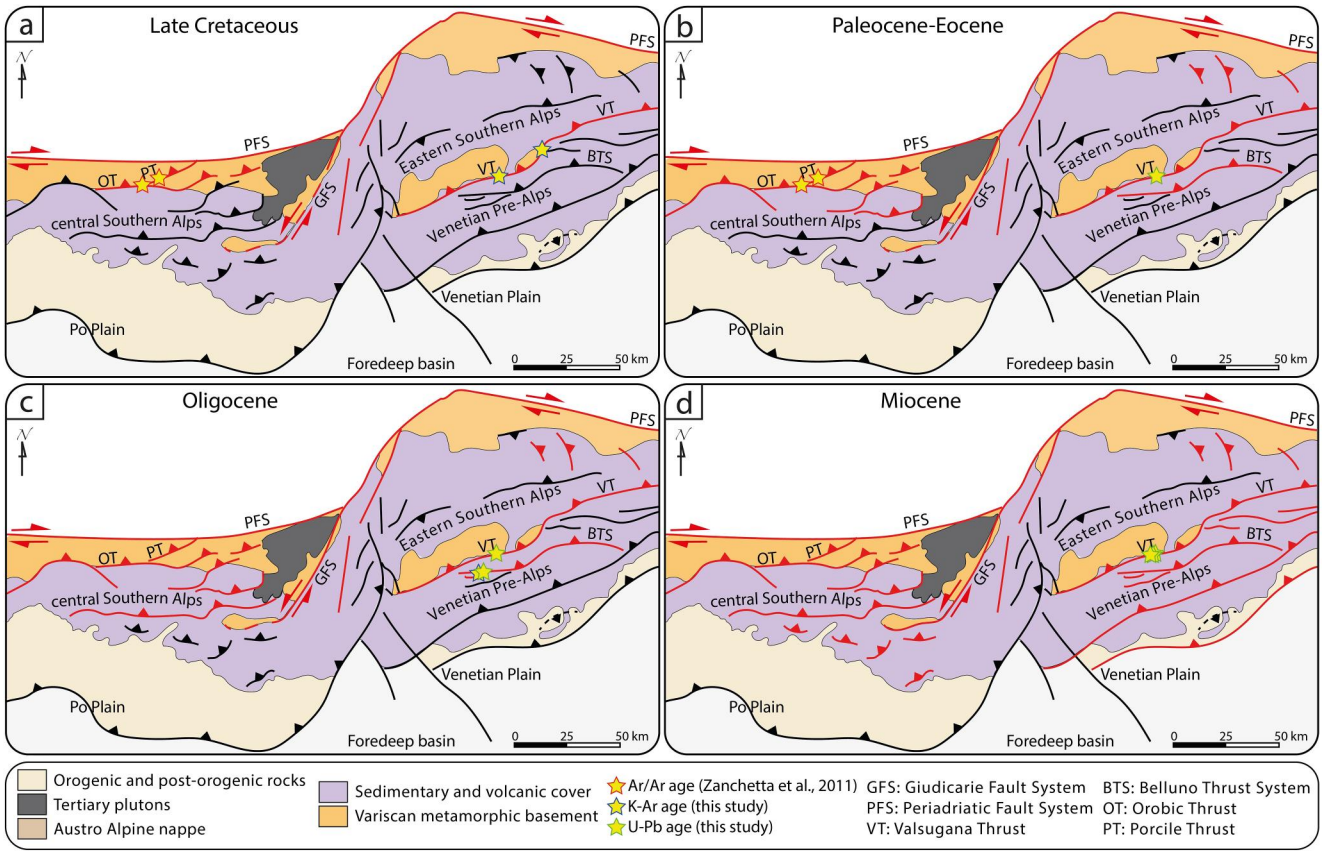

Figure 15. Model for the tectonic evolution of the central and Eastern Southern Alps (ESA). The model in map view refers to the present-day simplified geological and structural framework and shows the sequential activation (as red lines) of thrusts through time. The Late Cretaceous geochronological constraints in the ESA arise from structures associated with the Valsugana Thrust.

FTBs worldwide and it is generally reported as being greatly facilitated by the reactivation and inversion of inherited faults (e.g., Aldega et al., 2019). In this perspective, considering that the VT was active since Permian times (as suggested by the occurrence of Permian volcanics only to the north of the VT; Bosellini & Doglioni, 1986; Brandner et al., 2011; Castellarin & Vai, 1982; Selli, 1998), it is likely that the VT has acted as a long-lived crustal discontinuity that, following on a Permian nucleation, might have permitted the accommodation of also a Late Cretaceous shortening far-field stress. While folding, thrusting, and exhumation of the Variscan metamorphic basement are well known to have occurred during the Late Cretaceous in the cSA along the OT and PT (Fantoni et al., 2004; Zanchetta et al., 2011, 2015), our results are the first to report broadly coeval deformation also in the ESA (Figure 15a). Coeval and coaxial NW-SE compression and shortening during the Late Cretaceous in both the cSA and the ESA might have significant implications upon the first-order classic subdivision of the SA, which are traditionally divided into two sectors by the sinistral transpressive GFS (e.g., Castellarin et al., 2006). In detail, although the ESA have been generally interpreted as having formed since the Oligocene (e.g., Castellarin et al., 2006), our results suggest that the GFS would not represent a major structural divide separating two kinematically distinct domains (the cSA and ESA). On the contrary, they both would exhibit evidence of NW-SE shortening leading to a dominant SE vergence of the belt. As concluded by Zanchetta et al. (2015), our results confirm that both the ESA and the cSA were structured not only during the Cenozoic continental collision between Adria and Europe, but were initially shaped as the retro-wedge of the Alpine orogen by a complex pre-collisional and early subduction tectonic history of the European plate. However, while Late Cretaceous deformation in the cSA gave rise to folding, first-order thrusting through the ductile and brittle deformation regime (OT and PT), basement exhumation and erosion (e.g., Zanchetta et al., 2015), the coeval deformation in the ESA is so far only known to have caused incipient deformation localized at low structural

levels. Within this tectonic/structural scenario, the role of the GFS, which should be reevaluated as mentioned above, requires further investigations to better constrain its role within the overall tectonic evolution of the SA.

After its Late Cretaceous activation, the VT continued to localize deformation during Paleocene-Eocene times, when also the BTS began to accommodate shortening (Figures 14 and 15b). During the Oligocene, minor backthrusts formed, and the sedimentary cover was also deformed by folds that, after reaching a mature stage, were cut by punctuated slip events along the VT and BTS (Figure 15c). In the Miocene, the more external Moline and Tezze thrusts formed in the Venetian Pre-Alps, the BTS continued its activity, and the VT accommodated further slip at ∼15 and 10 Ma (Figures 14 and 15d). Further to the east, Eocene-Miocene deformation was accommodated by SW verging thrusts ascribed to the dynamics of the Dinaric belt (Doglioni, 1985, Figures 15b–15d). During the Late Miocene, the more external structures of the Venetian Pre-Alps (i.e., the Bassano-Maniago and Montello Thrusts) began their top-to-the SE propagation. At that time, the BTS became progressively inactive and the VT continued to accommodate out-of-sequence reactivation, as documented by a slip event constrained to ∼6 Ma (Figures 14 and 15e).

Our data confirm that the studied segment of the ESA accommodated NW-SE shortening and bulk top-to-the SE transport, which is kinematically coherent with the post-collisional (Miocene) Valsugana system of Castellarin and Cantelli (2000) and Castellarin et al. (2006).

In summary, we propose that the evolution of the ESA is the result of pre-, syn-, and post-collisional long-term and repeated deformation events. Hence, the post-collisional Miocene Valsugana system, as discussed in the literature, could only represent a partial archive of the long-lived and multiphase NW-SE orogenic shortening of the ESA. In this scenario, the post-collisional tectonic evolution of the ESA, which includes the Dinaric, Valsugana, and Schio-Vicenza structural systems proposed by Castellarin and Cantelli (2000) and Castellarin et al. (2006), might require some reconsideration. The lack of structures kinematically consistent with the post-collisional Dinaric and Schio-Vicenza systems in the studied portion of the ESA, however, prevents the possibility to elaborate more detailed considerations on the full post-collisional evolution of the ESA. Hence, further geochronological constraints from the entire ESA are needed in the future to generate an evolutionary model that can also account for the timing (e.g., initiation and longevity) and structural interaction modes among the different post-collisional systems of the ESA.

6. Conclusions

Our work provides the first absolute time constraints on fold and thrust development in the ESA, allowing us to shed new light on the complex and long-lived tectonic evolution of this portion of the SA. We dated to the Late Cretaceous the early activity of the VT, which is one of the major regional thrusts in the Alps and that was active for ∼72 Myr. The initiation of VT activity is interpreted as being associated with far-field stresses, when deformation first localized at low structural levels (i.e., within the metamorphic basement), and then continued through to the Late Miocene. The overall top-to-the-SE kinematics, coupled with geochronological constraints, indicates that the structural grain of the ESA reflects long-lasting NW-SE shortening within a scenario of out-of-sequence thrusting. New geochronological data provide constraints on the polyphase orogenic build-up of the entire belt of the SA, as suggested by the fact that the initiation of Alpine compression was synchronously recorded during the Late Cretaceous by the most internal south-verging thrusts along both the central and the eastern domains of the SA.

Acknowledgments
This research has been partially funded by the FAST project (Fault Architecture in Space and Time; PI: Giulio Viola), a research project funded by the Italian Ministry for University and Research (MUR) with the PRIN 2020 funding action (CUP J33C22000170001). E. Carminati and S. Tavani are thanked for fruitful comments. V. Moretto is warmly thanked for assistance during Rietveld refinement of X-ray patterns. This work benefited from fruitful and constructive reviews by the Editor, Sam Haines, Catherine Mottram, and an anonymous reviewer.

Data Availability Statement

Data can be found at Curzi, Cipriani, et al. (2024). U-Pb and XRD data of the Eastern Southern Alps–Curzi, Cipriani, et al. (2024) Tectonics. [dataset]. figshare. https://doi.org/10.6084/m9.figshare.25212734.

References

Aldega, L., Viola, G., Casas-Sainz, A., Marcén, M., Román-Berdiel, T., & van der Lelij, R. (2019). Unraveling multiple thermotectonic events accommodated by crustal-scale faults in Northern Iberia, Spain: Insights from K-Ar dating of clay gouges. *Tectonics*, *38*(10), 3629–3651. https://doi.org/10.1029/2019tc005585

Anderlini, L., Serpelloni, E., Tolomei, C., De Martini, P. M., Pezzo, G., Gualandi, A., & Spada, G. (2020). New insights into active tectonics and seismogenic potential of the Italian Southern Alps from vertical geodetic velocities. *Solid Earth*, *11*(5), 1681–1698. https://doi.org/10.5194/se-11-1681-2020

Anselmi, M., Govoni, A., De Gori, P., & Chiarabba, C. (2011). Seismicity and velocity structures along the south-Alpine thrust front of the Venetian Alps (NE-Italy). *Tectonophysics*, *513*(1–4), 37–48. https://doi.org/10.1016/j.tecto.2011.09.023

Barchi, M., Minelli, G., & Pialli, G. (1998). The CROP 03 profile: A synthesis of results on deep structures of the Northern Apennines. *Memorie della Societa Geologica Italiana*, *52*, 383–400.

Beaudoin, N. E., Lacombe, O., Hoareau, G., & Callot, J. P. (2022). How the geochemistry of syn-kinematic calcite cement depicts past fluid flow and assists structural interpretations: A review of concepts and applications in orogenic forelands. *Geological Magazine*, *159*(11–12), 2157–2190. https://doi.org/10.1017/s0016756822001327

Benedetti, L., Tapponnier, P., King, G. C., Meyer, B., & Manighetti, I. (2000). Growth folding and active thrusting in the Montello region, Veneto, northern Italy. *Journal of Geophysical Research*, *105*(B1), 739–766. https://doi.org/10.1029/1999jb900222

Bigi, G., Castellarin, A., Catalano, R., Coli, M., Cosentino, D., Dal Piaz, G. V., et al. (1989). *Synthetic structural-kinematic map of Italy*. C.N.R., Progetto Finalizzato Geodinamica, SELCA Firenze.

Bignami, C., Burrato, P., Cannelli, V., Chini, M., Falcucci, E., Ferretti, A., et al. (2012). Coseismic deformation pattern of the Emilia 2012 seismic sequence imaged by Radarsat-1 interferometry. *Annals of Geophysics*, *55*(4). https://doi.org/10.4401/ag-6157

Bilau, A., Bienveignant, D., Rolland, Y., Schwartz, S., Godeau, N., Guihou, A., et al. (2023). The Tertiary structuration of the Western Subalpine foreland deciphered by calcite-filled faults and veins. *Earth-Science Reviews*, *236*, 104270. https://doi.org/10.1016/j.earscirev.2022.104270

Bonadiman, C., Coltorti, M., & Siena, F. (1994). Petrogenesis and T-fO2 estimates of Mt. Monzoni complex (Central Dolomites, Southern Alps): A Triassic shoshonitic intrusion in a transcurrent geodynamic setting. *European Journal of Mineralogy*, *6*(6), 943–966. https://doi.org/10.1127/ejm/6/6/0943

Bosellini, A., & Doglioni, C. (1986). Inherited structures in the hangingwall of the Valsugana overthrust (Southern Alps, Northern Italy). *Journal of Structural Geology*, *8*(5), 581–583. https://doi.org/10.1016/0191-8141(86)90007-6

Bosellini, A., Gianolla, P., & Stefani, M. (2003). Geology of the dolomites. *Episodes Journal of International Geoscience*, *26*(3), 181–185. https://doi.org/10.18814/epiiugs/2003/v26i3/005

Bosellini, A., Masetti, D., & Sarti, M. (1981). A Jurassic "Tongue of the ocean" infilled with oolitic sands: The Belluno Trough, Venetian Alps, Italy. *Marine Geology*, *44*(1–2), 59–95. https://doi.org/10.1016/0025-3227(81)90113-4

Boullier, A. M., Fujimoto, K., Ohtani, T., Roman-Ross, G., Lewin, E., Ito, H., et al. (2004). Textural evidence for recent co-seismic circulation of fluids in the Nojima fault zone, Awaji island, Japan. *Tectonophysics*, *378*(3–4), 165–181. https://doi.org/10.1016/j.tecto.2003.09.006

Boyer, S. E., & Elliott, D. (1982). Thrust systems. *American Association of Petroleum Geology Bulletin*, *66*(9), 1196–1230. https://doi.org/10.1306/03b5a77d-16d1-11d7-8645000102c1865d

Brandner, R., Keim, L., & Adige, B. (2011). A 4-day geological field trip in the western dolomites. *Geology of the Alps*, *8*, 76–118.

Burbank, D. W., Puigdefàbregas, C. A. I., & Munoz, J. A. (1992). The chronology of the Eocene tectonic and stratigraphic development of the eastern Pyrenean foreland basin, northeast Spain. *Geological Society of America Bulletin*, *104*(9), 1101–1120. https://doi.org/10.1130/0016-7606(1992)104<1101:tcotet>2.3.co;2

Caputo, R., Poli, M. E., & Zanferrari, A. (2010). Neogene–Quaternary tectonic stratigraphy of the eastern Southern Alps, NE Italy. *Journal of Structural Geology*, *32*(7), 1009–1027. https://doi.org/10.1016/j.jsg.2010.06.004

Carboni, F., Viola, G., Aldega, L., van der Lelij, R., Brozzetti, F., & Barchi, M. R. (2020). K-Ar fault gouge dating of Neogene thrusting: The case of the siliciclastic deposits of the Trasimeno Tectonic Wedge (Northern Apennines, Italy). *Italian Journal of Geosciences*, *139*(2), 300–308. https://doi.org/10.3301/ijg.2020.06

Carminati, E., Aldega, L., Smeraglia, L., Scharf, A., Mattern, F., Albert, R., & Gerdes, A. (2020). Tectonic evolution of the northern Oman Mountains, Part of the Strait of Hormuz Syntaxis: New structural and paleothermal analyses and U-Pb dating of Synkinematic Calcite. *Tectonics*, *39*(4), e2019TC005936. https://doi.org/10.1029/2019tc005936

Carminati, E., & Doglioni, C. (2012). Alps vs. Apennines: The paradigm of a tectonically asymmetric Earth. *Earth-Science Reviews*, *112*(1–2), 67–96. https://doi.org/10.1016/j.earscirev.2012.02.004

Carminati, E., Lustrino, M., Cuffaro, M., & Doglioni, C. (2010). Tectonics, magmatism and geodynamics of Italy: What we know and what we imagine. *Journal of the Virtual Explorer*, *36*(8), 10–3809. https://doi.org/10.3809/jvirtex.2010.00226

Cassinis, G., Cortesogno, L., Gaggero, L., Perotti, C. R., & Buzzi, L. (2008). Permian to Triassic geodynamic and magmatic evolution of the Brescian Prealps (Eastern Lombardy, Italy). *Bollettino della Societa Geologica Italiana*, *127*(3), 501–518.

Castellarin, A., & Cantelli, L. (2000). Neo-Alpine evolution of the southern Eastern Alps. *Journal of Geodynamics*, *30*(1–2), 251–274. https://doi.org/10.1016/s0264-3707(99)00036-8

Castellarin, A., Cantelli, L., Fesce, A. M., Mercier, J. L., Picotti, V., Pini, G. A., et al. (1992). Alpine compressional tectonics in the Southern Alps. Relationships with the N-Apennines. *Annales Tectonicae*, *6*(1), 62–94.

Castellarin, A., Nicolich, R., Fantoni, R., Cantelli, L., Sella, M., & Selli, L. (2006). Structure of the lithosphere beneath the Eastern Alps (southern sector of the TRANSALP transect). *Tectonophysics*, *414*(1–4), 259–282. https://doi.org/10.1016/j.tecto.2005.10.013

Castellarin, A., Selli, L., Picotti, V., & Cantelli, L. (1998). Tettonismo e diapirismo medio Triassico delle Dolomiti. *Memorie della Societa Geologica Italiana*, *53*, 145–169.

Castellarin, A., & Vai, G. B. (1982). Introduzione alla geologia strutturale del Sudalpino. *Guida alla geologia del Sudalpino centro-orientale. Guide Geologiche Regionali della Società Geologica Italiana* (pp. 1–22).

Cavinato, G. P., & Celles, P. D. (1999). Extensional basins in the tectonically bimodal central Apennines fold-thrust belt, Italy: Response to corner flow above a subducting slab in retrograde motion. *Geology*, *27*(10), 955–958. https://doi.org/10.1130/0091-7613(1999)027<0955:ebittb>2.3.co;2

Cheloni, D., D'Agostino, N., & Selvaggi, G. (2014). Interseismic coupling, seismic potential, and earthquake recurrence on the southern front of the Eastern Alps (NE Italy). *Journal of Geophysical Research: Solid Earth*, *119*(5), 4448–4468. https://doi.org/10.1002/2014jb010954

Cipollari, P., & Cosentino, D. (1995). Miocene unconformities in the Central Apennines: Geodynamic significance and sedimentary basin evolution. *Tectonophysics*, *252*(1–4), 375–389. https://doi.org/10.1016/0040-1951(95)00088-7

Clauer, N. (2013). The K-Ar and 40Ar/39Ar methods revisited for dating fine-grained K-bearing clay minerals. *Chemical Geology*, *354*, 163–185. https://doi.org/10.1016/j.chemgeo.2013.05.030

Cozzi, A. (2002). Facies patterns of a tectonically-controlled Upper Triassic platform-slope carbonate depositional system (Carnian Prealps, Northeastern Italy). *Facies*, *47*(1), 151–178. https://doi.org/10.1007/bf02667711

Craddock, J. P., Nuriel, P., Kylander-Clark, A. R., Hacker, B. R., Luczaj, J., & Weinberger, R. (2022). Long-term (7 Ma) strain fluctuations within the Dead Sea transform system from high-resolution U-Pb dating of a calcite vein. *GSA Bulletin*, *134*(5–6), 1231–1246. https://doi.org/10.1130/b36000.1

Cruset, D., Vergés, J., Albert, R., Gerdes, A., Benedicto, A., Cantarero, I., & Travé, A. (2020). Quantifying deformation processes in the SE Pyrenees using U–Pb dating of fracture-filling calcites. *Journal of the Geological Society*, *177*(6), 1186–1196. https://doi.org/10.1144/jgs2020-014

Curzi, M., Aldega, L., Bernasconi, S. M., Berra, F., Billi, A., Boschi, C., et al. (2020a). Architecture and evolution of an extensionally-inverted thrust (Mt. Tancia Thrust, Central Apennines): Geological, structural, geochemical, and K–Ar geochronological constraints. *Journal of Structural Geology*, *136*, 104059. https://doi.org/10.1016/j.jsg.2020.104059

Curzi, M., Bernasconi, S. M., Billi, A., Boschi, C., Aldega, L., Franchini, S., et al. (2021). U-Pb age of the 2016 Amatrice earthquake causative fault (Mt. Gorzano, Italy) and paleo-fluid circulation during seismic cycles inferred from inter-and co-seismic calcite. *Tectonophysics*, *819*, 229076. https://doi.org/10.1016/j.tecto.2021.229076

Curzi, M., Billi, A., Carminati, E., Rossetti, F., Albert, R., Aldega, L., et al. (2020b). Disproving the presence of Paleozoic-Triassic metamorphic rocks on the Island of Zannone (central Italy): Implications for the early stages of the Tyrrhenian-Apennines tectonic evolution. *Tectonics*, *39*(12), e2020TC006296. https://doi.org/10.1029/2020tc006296

Curzi, M., Cipriani, A., Aldega, L., Billi, A., Carminati, E., Van der Lelij, R., et al. (2024). Architecture and permeability structure of the Sibillini Mts. Thrust and influence upon recent, extension-related seismicity in the central Apennines (Italy) through fault-valve behavior. *Geological Society of America Bulletin*, *136*(1–2), 3–26. https://doi.org/10.1130/B36616.1

Curzi, M., Viola, G., Zuccari, C., Aldega, L., Billi, A., Van der Lelij, R., et al. (2024). U-Pb and XRD data of the Eastern Southern Alps [Dataset]. figshare. https://doi.org/10.6084/m9.figshare.25212734

Curzi, M., Zuccari, C., Vignaroli, G., Degl'Innocenti, S., & Viola, G. (2023). Alpine transpression in the Passo Rolle area (Dolomites, Italy): New structural and paleostress constraints. *Italian Journal of Geosciences*, *142*(2), 1–17. https://doi.org/10.3301/ijg.2023.12

D'Adda, P., Zanchi, A., Bergomi, M., Berra, F., Malusà, M. G., Tunesi, A., & Zanchetta, S. (2011). Polyphase thrusting and dyke emplacement in the central Southern Alps (Northern Italy). *International Journal of Earth Sciences*, *100*(5), 1095–1113. https://doi.org/10.1007/s00531-010-0586-2

D'Agostino, N., Cheloni, D., Mantenuto, S., Selvaggi, G., Michelini, A., & Zuliani, D. (2005). Strain accumulation in the southern Alps (NE Italy) and deformation at the northeastern boundary of Adria observed by CGPS measurements. *Geophysical Research Letters*, *32*(19). https://doi.org/10.1029/2005gl024266

Danesi, S., Pondrelli, S., Salimbeni, S., Cavaliere, A., Serpelloni, E., Danecek, P., et al. (2015). Active deformation and seismicity in the Southern Alps (Italy): The Montello hill as a case study. *Tectonophysics*, *653*, 95–108. https://doi.org/10.1016/j.tecto.2015.03.028

DeCelles, P. G. (1994). Late Cretaceous-Paleocene synorogenic sedimentation and kinematic history of the Sevier thrust belt, northeast Utah and southwest Wyoming. *Geological Society of America Bulletin*, *106*(1), 32–56. https://doi.org/10.1130/0016-7606(1994)106<0032:lcpssa>2.3.co;2

Doglioni, C. (1985). The overthrusts in the Dolomites: Ramp-flat systems. *Eclogae Geologicae Helvetiae*, *78*(2), 335–350.

Doglioni, C. (1987). Tectonics of the Dolomites (southern Alps, northern Italy). *Journal of Structural Geology*, *9*(2), 181–193. https://doi.org/10.1016/0191-8141(87)90024-1

Doglioni, C. (1990). Thrust tectonics examples from the Venetian Alps. *Studi Geologici Camerti*, 117–129.

Doglioni, C. (1992). The Venetian Alps thrust belt. *Thrust tectonics*, 319–324. https://doi.org/10.1007/978-94-011-3066-0_29

Doglioni, C., & Bosellini, A. (1987). Eoalpine and mesoalpine tectonics in the Southern Alps. *Geologische Rundschau*, *76*(3), 735–754. https://doi.org/10.1007/bf01821061

Doglioni, C., & Carminati, E. (2008). Structural styles and Dolomites field trip. *Memorie Descrittive della Carta Geologica d'Italia*, *82*, 1–299.

Doglioni, C., & Neri, C. (1988). Anisian tectonics in the Passo Rolle area. *Rendiconti della Societa Geologica Italiana*, *11*, 197–204.

Dunkl, I., Picotti, V., Selli, L., Castellarin, A., & Fritsch, W. (1996). Low temperature thermal history of the dolomites. Preliminary results. 78° Summer Meeting of the It. Geol. Soc. (BZ), 16–18/9.

Evans, M. A., & Fischer, M. P. (2012). On the distribution of fluids in folds: A review of controlling factors and processes. *Journal of Structural Geology*, *44*, 2–24. https://doi.org/10.1016/j.jsg.2012.08.003

Fantoni, R., Bersezio, R., & Forcella, F. (2004). Alpine structure and deformation chronology at the southern Alps-Po plain border in Lombardy. *Bollettino della Societa Geologica Italiana*, *123*(3), 463–476.

Galadini, F., Poli, M. E., & Zanferrari, A. (2005). Seismogenic sources potentially responsible for earthquakes with M≥ 6 in the Eastern Southern Alps (Thiene-Udine sector, NE Italy). *Geophysical Journal International*, *161*(3), 739–762. https://doi.org/10.1111/j.1365-246x.2005.02571.x

Goodfellow, B. W., Viola, G., Bingen, B., Nuriel, P., & Kylander-Clark, A. R. (2017). Palaeocene faulting in SE Sweden from U–Pb dating of slickenfibre calcite. *Terra Nova*, *29*(5), 321–328. https://doi.org/10.1111/ter.12280

Haines, S. H., & van der Pluijm, B. A. (2023). Fault gouge dating in the Spanish Pyrenees: Fault ages, thrust propagation sequence, wall-rock provenance, and thermal constraints. *Tectonics*, *42*(2), e2022TC007251. https://doi.org/10.1029/2022tc007251

Handy, M. R., Schmid, S. M., Bousquet, R., Kissling, E., & Bernoulli, D. (2010). Reconciling plate-tectonic reconstructions of Alpine Tethys with the geological–geophysical record of spreading and subduction in the Alps. *Earth-Science Reviews*, *102*(3–4), 121–158. https://doi.org/10.1016/j.earscirev.2010.06.002

Hansman, R. J., Albert, R., Gerdes, A., & Ring, U. (2018). Absolute ages of multiple generations of brittle structures by U-Pb dating of calcite. *Geology*, *46*(3), 207–210. https://doi.org/10.1130/g39822.1

Harding, T., & Lowell, J. D. (1979). Structural styles, their plate-tectonic habitats, and hydrocarbon traps in petroleum provinces. *American Association of Petroleum Geology Bulletin*, *63*(7), 1016–1058. https://doi.org/10.1306/2f9184b4-16ce-11d7-8645000102c1865d

Heberer, B., Reverman, R. L., Fellin, M. G., Neubauer, F., Dunkl, I., Zattin, M., et al. (2017). Postcollisional cooling history of the eastern and southern Alps and its linkage to Adria indentation. *International Journal of Earth Sciences*, *106*(5), 1557–1580. https://doi.org/10.1007/s00531-016-1367-3

Hudec, M. R., & Davis, G. A. (1989). Out-of-sequence thrust faulting and duplex formation in the Lewis thrust system, Spot Mountain, southeastern Glacier National Park, Montana. *Canadian Journal of Earth Sciences*, *26*(11), 2356–2364. https://doi.org/10.1139/e89-201

Keim, L., & Stingl, V. (2000). Lithostratigraphy and facies architecture of the Oligocene conglomerates at Monte Parei (Fanes, dolomites, Italy). *Rivista Italiana di Paleontologia e Stratigrafia*, *106*, 123–131.

Lacombe, O., & Beaudoin, N. E. (2023). Timing, sequence, duration and rate of deformation in fold-and-thrust belts: A review of traditional approaches and recent advances from absolute dating (K–Ar illite/U–Pb calcite) of brittle structures. *Comptes Rendus Geoscience*, *356*(S2), 1–28. https://doi.org/10.5802/crgeos.218

Lacombe, O., Beaudoin, N. E., Hoareau, G., Labeur, A., Pecheyran, C., & Callot, J. P. (2021). Dating folding beyond folding, from layer-parallel shortening to fold tightening, using mesostructures: Lessons from the Apennines, Pyrenees, and Rocky Mountains. *Solid Earth*, *12*(10), 2145–2157. https://doi.org/10.5194/se-12-2145-2021

Lacombe, O., & Bellahsen, N. (2016). Thick-skinned tectonics and basement-involved fold–thrust belts: Insights from selected Cenozoic orogens. *Geological Magazine*, *153*(5–6), 763–810. https://doi.org/10.1017/s0016756816000078

Lacombe, O., Lavè, J., Roure, F. M., & Verges, J. (2007). Thrust belts and foreland basins: From fold kinematics to hydrocarbon systems. In *Frontiers in Earth Sciences series* (Vol. 308). Springer Science & Business Media.

Looser, N., Madritsch, H., Guillong, M., Laurent, O., Wohlwend, S., & Bernasconi, S. M. (2021). Absolute age and temperature constraints on deformation along the basal décollement of the Jura fold-and-thrust belt from carbonate U-Pb dating and clumped isotopes. *Tectonics*, *40*(3), e2020TC006439. https://doi.org/10.1029/2020tc006439

Lustrino, M., Abbas, H., Agostini, S., Caggiati, M., Carminati, E., & Gianolla, P. (2019). Origin of Triassic magmatism of the southern Alps (Italy): Constraints from geochemistry and Sr-Nd-Pb isotopic ratios. *Gondwana Research*, *75*, 218–238. https://doi.org/10.1016/j.gr.2019.04.011

Masetti, D., Fantoni, R., Romano, R., Sartorio, D., & Trevisani, E. (2012). Tectonostratigraphic evolution of the Jurassic extensional basins of the Eastern Southern Alps and Adriatic foreland based on an integrated study of surface and subsurface data. *American Association of Petroluem Geology Bulletin*, *96*(11), 2065–2089. https://doi.org/10.1306/03091211087

Massironi, M., Preto, N., & Zampieri, D. (2007). *Carta geologica della provincia di Trento. Tavola 45 III – S. Martino di Castrozza. 1:25,000*. Provincia Autonoma di Trento, Servizio Geologico.

Mietto, P., Avanzini, M., Belvedere, M., Bernardi, M., Dalla Vecchia, F. M., Porchetti, S. D. O., et al. (2020). Triassic tetrapod ichnofossils from Italy: The state of the art. *Journal of Mediterranean Earth Sciences*, *12*, 83–136.

Mitra, S. (1986). Duplex structures and imbricate thrust systems: Geometry, structural position, and hydrocarbon potential. *American Association of Petroluem Geology Bulletin*, *70*(9), 1087–1112. https://doi.org/10.1306/94886a7e-1704-11d7-8645000102c1865d

Morelli, C., Marocchi, M., Moretti, A., Bargossi, G. M., Gasparotto, G., De Waele, B., et al. (2012). Volcanic stratigraphy and radiometric age constraints at the northern margin of a mega-caldera system: Athesian Volcanic Group (Southern Alps, Italy). *Geológica Acta*, *11*, 51–67.

Morley, C. K. (1988). Out-of-sequence thrusts. *Tectonics*, *7*(3), 539–561. https://doi.org/10.1029/tc007i003p00539

Mottram, C. M., Kellett, D. A., Barresi, T., Zwingmann, H., Friend, M., Todd, A., & Percival, J. B. (2020). Syncing fault rock clocks: Direct comparison of U-Pb carbonate and K-Ar illite fault dating methods. *Geology*, *48*(12), 1179–1183. https://doi.org/10.1130/g47778.1

Müller, W. (2003). Strengthening the link between geochronology, textures and petrology. *Earth and Planetary Science Letters*, *206*(3–4), 237–251. https://doi.org/10.1016/s0012-821x(02)01007-5

Müller, W., Prosser, G., Mancktelow, N. S., Villa, I. M., Kelley, S. P., Viola, G., & Oberli, F. (2001). Geochronological constraints on the evolution of the Periadriatic Fault System (Alps). *International Journal of Earth Sciences*, *90*(3), 623–653. https://doi.org/10.1007/s005310000187

Munoz-Lopez, D., Cruset, D., Vergés, J., Cantarero, I., Benedicto, A., Mangenot, X., et al. (2022). Spatio-temporal variation of fluid flow behavior along a fold: The Bóixols-Sant Corneli anticline (southern Pyrenees) from U–Pb dating and structural, petrographic and geochemical constraints. *Marine and Petroleum Geology*, *143*, 105788. https://doi.org/10.1016/j.marpetgeo.2022.105788

Nuriel, P., Weinberger, R., Kylander-Clark, A. R. C., Hacker, B. R., & Craddock, J. P. (2017). The onset of the Dead Sea transform based on calcite age-strain analyses. *Geology*, *45*(7), 587–590. https://doi.org/10.1130/g38903.1

Palacios-García, N. B., Fitz-Díaz, E., Stockli, L. D., & Stockli, D. F. (2023). U–Pb calcite dating of brittle deformation in Permian carbonates within the Chicomuselo fold and thrust belt, SE Mexico. *Journal of Structural Geology*, *171*, 104863. https://doi.org/10.1016/j.jsg.2023.104863

Pană, D. I., & van der Pluijm, B. A. (2015). Orogenic pulses in the Alberta Rocky Mountains: Radiometric dating of major faults and comparison with the regional tectono-stratigraphic record. *Bulletin*, *127*(3–4), 480–502. https://doi.org/10.1130/b31069.1

Pevear, D. R. (1999). Illite and hydrocarbon exploration. *Proceedings of the National Academy of Sciences*, *96*(7), 3440–3446. https://doi.org/10.1073/pnas.96.7.3440

Picotti, V., & Cobianchi, M. (2017). Jurassic stratigraphy of the Belluno basin and Friuli platform: A perspective on far-field compression in the Adria passive margin. *Swiss Journal of Geosciences*, *110*(3), 833–850. https://doi.org/10.1007/s00015-017-0280-5

Picotti, V., Romano, M. A., Ponza, A., Guido, F. L., & Peruzza, L. (2022). The Montello thrust and the active mountain front of the Eastern Southern Alps (northeast Italy). *Tectonics*, *41*(12), e2022TC007522. https://doi.org/10.1029/2022tc007522

Poli, M. E., & Zanferrari, A. (1992). The Agordo basement (NE Italy): A 500 Ma-long geological record in the Southalpine crust. *IGCP*, *276*, 283–296.

Roberts, N. M., & Holdsworth, R. E. (2022). Timescales of faulting through calcite geochronology: A review. *Journal of Structural Geology*, *158*, 104578. https://doi.org/10.1016/j.jsg.2022.104578

Roberts, N. M., Žák, J., Vacek, F., & Sláma, J. (2021). No more blind dates with calcite: Fluid-flow vs. fault-slip along the Očkov thrust, Prague Basin. *Geoscience Frontiers*, *12*(4), 101143. https://doi.org/10.1016/j.gsf.2021.101143

Schmid, S. M., Aebli, H. R., Heller, F., & Zingg, A. (1989). The role of the Periadriatic Line in the tectonic evolution of the Alps. *Geological Society, London, Special Publications*, *45*(1), 153–171. https://doi.org/10.1144/gsl.sp.1989.045.01.08

Schmid, S. M., Bernoulli, D., Fügenschuh, B., Matenco, L., Schefer, S., Schuster, R., et al. (2008). The alpine-Carpathian-Dinaridic orogenic system: Correlation and evolution of tectonic units. *Swiss Journal of Geosciences*, *101*(1), 139–183. https://doi.org/10.1007/s00015-008-1247-3

Schönborn, G. (1999). Balancing cross sections with kinematic constraints: The Dolomites (northern Italy). *Tectonics*, *18*(3), 527–545. https://doi.org/10.1029/1998tc900018

Selli, L. (1998). IL lineamento della Valsugana fra Trento e Cima d'Asta: Cinematica neogenica ed eredità strutturali permo-mesozoiche nel quadro evolutivo del Sudalpino orientale (NE-Italia). *Memorie della Societa Geologica Italiana*, *53*, 503–541.

Serpelloni, E., Vannucci, G., Anderlini, L., & Bennett, R. A. (2016). Kinematics, seismotectonics and seismic potential of the eastern sector of the European Alps from GPS and seismic deformation data. *Tectonophysics*, *688*, 157–181. https://doi.org/10.1016/j.tecto.2016.09.026

Sibson, R. H. (1994). Crustal stress, faulting and fluid flow. *Geological Society, London, Special Publications*, *78*(1), 69–84. https://doi.org/10.1144/gsl.sp.1994.078.01.07

Sibson, R. H., Moore, J. M. M., & Rankin, A. H. (1975). Seismic pumping—A hydrothermal fluid transport mechanism. *Journal of the Geological Society*, *131*(6), 653–659. https://doi.org/10.1144/gsjgs.131.6.0653

Sieberer, A.-K., Willingshofer, E., Klotz, T., Ortner, H., & Pomella, H. (2023). Inversion of extensional basins parallel and oblique to their boundaries: Inferences from analogue models and field observations from the dolomites Indenter, European eastern southern Alps. *Solid Earth*, *14*(7), 647–681. https://doi.org/10.5194/se-14-647-2023

Sloman, L. E. (1989). Triassic shoshonites from the dolomites, northern Italy: Alkaline arc rocks in a strike-slip setting. *Journal of Geophysical Research*, *94*(B4), 4655–4666. https://doi.org/10.1029/jb094ib04p04655

Smeraglia, L., Aldega, L., Billi, A., Carminati, E., Di Fiore, F., Gerdes, A., et al. (2019). Development of an intrawedge tectonic mélange by out-of-sequence thrusting, buttressing, and intraformational rheological contrast, Mt. Massico ridge, Apennines, Italy. *Tectonics*, *38*(4), 1223–1249. https://doi.org/10.1029/2018tc005243

Smeraglia, L., Looser, N., Fabbri, O., Choulet, F., Guillong, M., & Bernasconi, S. M. (2021). U-Pb dating of middle Eocene-middle Pleistocene multiple tectonic pulses in the Alpine foreland. *Journal of Geophysical Research: Solid Earth*, 1–14. https://doi.org/10.5194/se-2021-2

Stefani, C., Fellin, M. G., Zattin, M., Zuffa, G. G., Dalmonte, C., Mancin, N., & Zanferrari, A. (2007). Provenance and paleogeographic evolution in a multi-source foreland: The Cenozoic Venetian–Friulian basin (NE Italy). *Journal of Sedimentary Research*, *77*(11), 867–887. https://doi.org/10.2110/jsr.2007.083

Tavani, S., Smeraglia, L., Fabbi, S., Aldega, L., Sabbatino, M., Cardello, G. L., et al. (2023). Timing, thrusting mode, and negative inversion along the Circeo thrust, Apennines, Italy: How the accretion-to-extension transition operated during slab rollback. *Tectonics*, *42*(6), e2022TC007679. https://doi.org/10.1029/2022tc007679

Tavani, S., Storti, F., Lacombe, O., Corradetti, A., Muñoz, J. A., & Mazzoli, S. (2015). A review of deformation pattern templates in foreland basin systems and fold-and-thrust belts: Implications for the state of stress in the frontal regions of thrust wedges. *Earth-Science Reviews*, *141*, 82–104. https://doi.org/10.1016/j.earscirev.2014.11.013

Torgersen, E., Viola, G., Zwingmann, H., & Henderson, I. H. (2015). Inclined K–Ar illite age spectra in brittle fault gouges: Effects of fault reactivation and wall-rock contamination. *Terra Nova*, *27*(2), 106–113. https://doi.org/10.1111/ter.12136

Trombetta, G., & Bottoli, S. (1998). Tettonica e stratigrafia medio-triassica nel gruppo Col Rossi-Porta Vescovo (Dolomiti occidentali). *Memorie della Societa Geologica Italiana*, *53*, 325–339.

Van der Pluijm, B. A., Hall, C. M., Vrolijk, P. J., Pevear, D. R., & Covey, M. C. (2001). The dating of shallow faults in the Earth's crust. *Nature*, *412*(6843), 172–175. https://doi.org/10.1038/35084053

Venzo, S. (1939). Nuovo lembo tortoniano strizzato tra Ie filladi ed il perrniano a Strigno di Valsugana (Trentino meridionale orientale). *Bollettino della Societa Geologica Italiana*, *58*(1), 175–185.

Viganò, A., Scafidi, D., Ranalli, G., Martin, S., Della Vedova, B., & Spallarossa, D. (2015). Earthquake relocations, crustal rheology, and active deformation in the central–eastern Alps (N Italy). *Tectonophysics*, *661*, 81–98. https://doi.org/10.1016/j.tecto.2015.08.017

Vignaroli, G., Rossetti, F., Petracchini, L., Argante, V., Bernasconi, S. M., Brilli, M., et al. (2022). Middle Pleistocene fluid infiltration with 10–15 ka recurrence within the seismic cycle of the active Monte Morrone Fault System (central Apennines, Italy). *Tectonophysics*, *827*, 229269. https://doi.org/10.1016/j.tecto.2022.229269

Vignaroli, G., Viola, G., Diamanti, R., Zuccari, C., Garofalo, P. S., Bonini, S., & Selli, L. (2020). Multistage strain localisation and fluid-assisted cataclasis in carbonate rocks during the seismic cycle: Insights from the Belluno Thrust (Eastern Southern Alps, Italy). *Journal of Structural Geology*, *141*, 104216. https://doi.org/10.1016/j.jsg.2020.104216

Viola, G., Mancktelow, N. S., & Seward, D. (2001). Late Oligocene- Neogene evolution of Europe-Adria collision: New structural and geochronological evidence from the Giudicarie Fault System (Italian eastern Alps). *Tectonics*, *20*(6), 999–1020. https://doi.org/10.1029/2001tc900021

Viola, G., Musumeci, G., Mazzarini, F., Tavazzani, L., Curzi, M., Torgersen, E., et al. (2022). Structural characterization and K–Ar illite dating of reactivated, complex and heterogeneous fault zones: Lessons from the Zuccale fault, northern Apennines. *Solid Earth*, *13*(8), 1327–1351. https://doi.org/10.5194/se-13-1327-2022

Viola, G., Scheiber, T., Fredin, O., Zwingmann, H., Margreth, A., & Knies, J. (2016). Deconvoluting complex structural histories archived in brittle fault zones. *Nature Communications*, *7*(1), 13448. https://doi.org/10.1038/ncomms13448

Viola, G., Torgersen, E., Mazzarini, F., Musumeci, G., van der Lelij, R., Schönenberger, J., & Garofalo, P. S. (2018). New constraints on the evolution of the inner northern Apennines by K-Ar dating of late Miocene-early Pliocene compression on the island of Elba, Italy. *Tectonics*, *37*(9), 3229–3243. https://doi.org/10.1029/2018tc005182

Viola, G., Zwingmann, H., Mattila, J., & Käpyaho, A. (2013). K-Ar illite age constraints on the Proterozoic formation and reactivation history of a brittle fault in Fennoscandia. *Terra Nova*, *25*(3), 236–244. https://doi.org/10.1111/ter.12031

Vrolijk, P., & van der Pluijm, B. A. (1999). Clay gouge. *Journal of Structural Geology*, *21*(8–9), 1039–1048. https://doi.org/10.1016/s0191-8141(99)00103-0

York, D., Evensen, N. M., Martínez, M. L., & De Basabe Delgado, J. (2004). Unified equations for the slope, intercept, and standard errors of the best straight line. *American Journal of Physics*, *72*(3), 367–375. https://doi.org/10.1119/1.1632486

Zanchetta, S., D'Adda, P., Zanchi, A., Barberini, V., & Villa, I. M. (2011). Cretaceous-Eocene compression in the central Southern Alps (N Italy) inferred from 40Ar/39Ar dating of pseudotachylytes along regional thrust faults. *Journal of Geodynamics*, *51*(4), 245–263. https://doi.org/10.1016/j.jog.2010.09.004

Zanchetta, S., Malusà, M. G., & Zanchi, A. (2015). Precollisional development and Cenozoic evolution of the Southalpine retrobelt (European Alps). *Lithosphere*, *7*(6), 662–681.

Zattin, M., Cuman, A., Fantoni, R., Martin, S., Scotti, P., & Stefani, C. (2006). From Middle Jurassic heating to Neogene cooling: The thermochronological evolution of the southern Alps. *Tectonophysics*, *414*(1–4), 191–202. https://doi.org/10.1016/j.tecto.2005.10.020

Zattin, M., Stefani, C., & Martin, S. (2003). Detrital fission-track analysis and sedimentary petrofacies as keys of alpine exhumation: The example of the Venetian foreland (European southern Alps, Italy). *Journal of Sedimentary Research*, *73*(6), 1051–1061. https://doi.org/10.1306/051403731051

Zuccari, C., Vignaroli, G., & Viola, G. (2021). Geological map of the San Donato–Costa thrust zone, Belluno thrust system, eastern southern Alps (northern Italy). *Journal of Maps*, *17*(2), 337–347. https://doi.org/10.1080/17445647.2021.1946444

Zuccari, C., Viola, G., Curzi, M., Aldega, L., & Vignaroli, G. (2022). What steers the "folding to faulting" transition in carbonate-dominated seismic fold-and-thrust belts? New insights from the eastern southern Alps (northern Italy). *Journal of Structural Geology*, *157*, 104560. https://doi.org/10.1016/j.jsg.2022.104560

Zwingmann, H., Offler, R., Wilson, T., & Cox, S. F. (2004). K–Ar dating of fault gouge in the northern Sydney basin, NSW, Australia—Implications for the breakup of Gondwana. *Journal of Structural Geology*, *26*(12), 2285–2295. https://doi.org/10.1016/j.jsg.2004.03.007

References From the Supporting Information

Clauer, N., & Chaudhuri, S. (1995). *Clays in crustal environments: Isotope tracing and dating* (p. 359). Springer-Verlag.

D'Alberto, L., Boz, A., & Doglioni, C. (1995). Structure of the vette Feltrine (Eastern Southern Alps). *Memorie di Scienze Geologiche*, *47*, 189–199.

Doebelin, N., & Kleeberg, R. (2015). Profex: A graphical user interface for the Rietveld refinement program BGMN. *Journal of Applied Crystallography*, *48*(5), 1573–1580. https://doi.org/10.1107/s1600576715014685

Fuhrmann, U., Lippolt, H. J., & Hess, J. C. (1987). Examination of some proposed K-Ar standards: 40Ar39Ar analyses and conventional K/Ar data: Chemical geology. *Isotope Geoscience Section*, *66*(1–2), 41–51. https://doi.org/10.1016/0168-9622(87)90027-3

Hill, C. A., Polyak, V. J., Asmerom, Y., & Provencio, P. (2016). Constraints on a Late Cretaceous uplift, denudation, and incision of the Grand Canyon region, southwestern Colorado Plateau, USA, from U-Pb dating of lacustrine limestone. *Tectonics*, *35*(4), 896–906. https://doi.org/10.1002/2016tc004166

Kylander-Clark, A. R. C. (2020). Expanding the limits of laser-ablation U-Pb calcite geochronology. *Geochronology*, *2*, 343–354. https://doi.org/10.5194/gchron-2-343-2020

Lee, J. Y., Marti, K., Severinghaus, J. P., Kawamura, K., Yoo, H. S., Lee, J. B., & Kim, J. S. (2006). A redetermination of the isotopic abundances of atmospheric Arc. *Geochimica et Cosmochimica Acta*, *70*(17), 4507–4512. https://doi.org/10.1016/j.gca.2006.06.1563

Nuriel, P., Wotzlaw, J. F., Ovtcharova, M., Vaks, A., Stremtan, C., Šala, M., et al. (2021). The use of ASH-15 flowstone as a matrix-matched reference material for laser-ablation U-Pb geochronology of calcite. *Geochronology*, *3*(1), 35–47. https://doi.org/10.5194/gchron-3-35-2021

Pagel, M., Bonifacie, M., Schneider, D. A., Gautheron, C., Brigaud, B., Calmels, D., et al. (2018). Improving paleohydrological and diagenetic reconstructions in calcite veins and breccia of a sedimentary basin by combining Δ47 temperature, δ18Owater and U-Pb age. *Chemical Geology*, *481*, 1–17. https://doi.org/10.1016/j.chemgeo.2017.12.026

Paton, C., Hellstrom, J., Paul, B., Woodhead, J., & Hergt, J. (2011). Iolite: Freeware for the visualisation and processing of mass spectrometric data. *Journal of Analytical Atomic Spectrometry*, *26*(12), 2508–2518. https://doi.org/10.1039/c1ja10172b

Roberts, N. M. W., Rasbury, E. T., Parrish, R. R., Smith, C. J., Horstwood, M. S. A., & Condon, D. J. (2017). A calcite reference material for LA-ICP-MS U-Pb geochronology. *Geochemistry, Geophysics, Geosystems*, *18*(7), 2807–2814. https://doi.org/10.1002/2016GC006784

Schumacher, E. (1975). Herstellung von 99, 9997% 38Ar für die 40K/40Ar Geochronologie. *Geochronologia Chimia*, *24*, 441–442.

Steiger, R., & Jäger, E. (1977). Subcommission on geochronology: Convention on the use of decay constants in geo-and cosmochronology. *Earth and Planetary Science Letters*, *36*(3), 359–362. https://doi.org/10.1016/0012-821x(77)90060-7